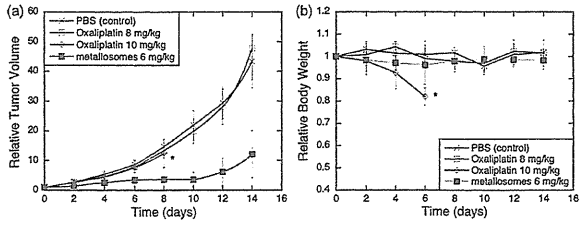

Figure 4. Antitumor activity of metallosomes through i.v. injection. (a) Relative tumor volume. (b) Relative body weight: oxaliplatin at 8 and 10 mg/kg and metallosomes at 6 mg/kg. Day 0 is the first day of injection. *Toxic death 6/6 mice. Data are mean ± SD of $n = 6$.

the high accumulation of drug in the tumor tissue without showing significant body weight loss (Figure 4b). The ability of metallosomes to load and deliver multiple therapeutic agents presents enormous possibilities for the design of new therapeutic strategies, such as loading different chemotherapeutic agents for improved combination chemotherapy or diagnosis agents for real-time monitoring of the therapeutic response.

The simple construction of metallosomes in water without use of organic solvents allows encapsulation of fragile bioactive compounds, and the observed *in vitro* and *in vivo* performance of the metallosomes against cancer offers a promising platform for the development of nanocarriers for versatile application. The tunable multifunctionality of block copolymers and the use of diverse metal coordination bond to assemble the vesicles will provide a method for creating smart carriers enabling both diagnosis and therapy, thereby reducing the complexity of multidrug administration.

■ ASSOCIATED CONTENT

Ⓢ Supporting Information

Materials and methods, TEM images of the assemblies prepared from PEG-PLGA-Chole or PEGasus-PLGA and DACHPt, molecular modeling of DACHPt/PLGA, and an additional table summarizing the *in vitro* cytotoxicity results. This material is available free of charge via the Internet at http://pubs.acs.org.

■ AUTHOR INFORMATION

Corresponding Author

kataoka@bmw.t.u-tokyo.ac.jp

Author Contributions

‖These authors contributed equally.

Notes

The authors declare no competing financial interest.

■ ACKNOWLEDGMENTS

This research was partly supported by Grant-in-Aid for Scientific Research on Priority Area "Cancer" from The Ministry of Education, Culture, Sports, Science and Technology, Japan, and by the Japan Society for the Promotion of Science (JSPS) through its "Funding Program for World-Leading Innovative R&D on Science and Technology (FIRST Program)."

■ REFERENCES

(1) Luo, L. B.; Eisenberg, A. *J. Am. Chem. Soc.* **2001**, *123*, 1012.
(2) Discher, D. E.; Eisenberg, A. *Science* **2002**, *297*, 967.
(3) Antonietti, M.; Forster, S. *Adv. Mater.* **2003**, *15*, 1323.
(4) Azzam, T.; Eisenberg, A. *Angew. Chem., Int. Ed.* **2006**, *45*, 7443.
(5) Christian, D. A.; Tian, A. W.; Ellenbroek, W. G.; Levental, I.; Rajagopal, K.; Janmey, P. A.; Liu, A. J.; Baumgart, T.; Discher, D. E. *Nat. Mater.* **2009**, *8*, 843.
(6) Meng, F. H.; Zhong, Z. Y.; Feijen, J. *Biomacromolecules* **2009**, *10*, 197.
(7) Zhang, L. F.; Yu, K.; Eisenberg, A. *Science* **1996**, *272*, 1777.
(8) Koide, A.; Kishimura, A.; Osada, K.; Jang, W. D.; Yamasaki, Y.; Kataoka, K. *J. Am. Chem. Soc.* **2006**, *128*, 5988.
(9) Anraku, Y.; Kishimura, A.; Oba, M.; Yamasaki, Y.; Kataoka, K. *J. Am. Chem. Soc.* **2010**, *132*, 1631.
(10) Kidani, Y.; Inagaki, K.; Iigo, M.; Hoshi, A.; Kuretani, K. *J. Med. Chem.* **1978**, *21*, 1315.
(11) Ibrahim, A.; Hirschfeld, S.; Cohen, M. H.; Griebel, D. J.; Williams, G. A.; Pazdur, R. *Oncologist* **2004**, *9*, 8.
(12) Nagasawa, M.; Holtzer, A. *J. Am. Chem. Soc.* **1964**, *86*, 538.
(13) Flory, P. J. *Proc. R. Soc. London, Ser. A* **1956**, *234*, 73.
(14) Parry, D. A.; Elliott, A. *Nature* **1965**, *206*, 616.
(15) Bellomo, E. G.; Wyrsta, M. D.; Pakstis, L.; Pochan, D. J.; Deming, T. J. *Nat. Mater.* **2004**, *3*, 244.
(16) Rodriguez-Hernandez, J.; Lecommandoux, S. *J. Am. Chem. Soc.* **2005**, *127*, 2026.
(17) Goodby, J. W. *Liq. Cryst.* **1998**, *24*, 25.
(18) Klok, H. A.; Hwang, J. J.; Iyer, S. N.; Stupp, S. I. *Macromolecules* **2002**, *35*, 746.
(19) Nishiyama, N.; Yokoyama, M.; Aoyagi, T.; Okano, T.; Sakurai, Y.; Kataoka, K. *Langmuir* **1999**, *15*, 377.
(20) Matsumura, Y.; Maeda, H. *Cancer Res.* **1986**, *46*, 6387.
(21) Cabral, H.; Nishiyama, N.; Kataoka, K. *J. Controlled Release* **2007**, *121*, 146.

Smart Multilayered Assembly for Biocompatible siRNA Delivery Featuring Dissolvable Silica, Endosome-Disrupting Polycation, and Detachable PEG

Tomoya Suma,[†] Kanjiro Miyata,[†,*] Yasutaka Anraku,[§] Sumiyo Watanabe,[‡] R. James Christie,[‡] Hiroyasu Takemoto,[§] Momoko Shioyama,[§] Noha Gouda,[†] Takehiko Ishii,[†] Nobuhiro Nishiyama,[‡] and Kazunori Kataoka[†,‡,§,⊥,*]

[†]Department of Bioengineering, Graduate School of Engineering, The University of Tokyo, 7-3-1 Hongo, Bunkyo-ku, Tokyo 113-8656, Japan, [‡]Center for Disease Biology and Integrative Medicine, Graduate School of Medicine, The University of Tokyo, 7-3-1 Hongo, Bunkyo-ku, Tokyo 113-0033, Japan, [§]Department of Materials Engineering, Graduate School of Engineering, The University of Tokyo, 7-3-1 Hongo, Bunkyo-ku, Tokyo 113-8656, Japan, and [⊥]Center for NanoBio Integration, The University of Tokyo, 7-3-1 Hongo, Bunkyo-ku, Tokyo 113-8656, Japan

ABSTRACT Multifunctional delivery systems of small interfering RNA (siRNA) are needed to overcome the intrinsic biological barriers toward efficient gene silencing in the cell cytoplasm. In this report, a smart multilayered assembly (SMA) was fabricated by a layer-by-layer method with polyionic materials. The SMA was designed to feature a siRNA-loaded core, a transiently core-stabilizing silica interlayer, an endosome-disrupting polycation interlayer, and a biocompatible poly(ethylene glycol) (PEG) shell with reductive environment-responsive detachability. The SMA was confirmed to be approximately 160 nm in size with narrow distribution and spherical morphology by DLS and TEM analyses. The PEG detachability of the SMA based on disulfide cleavage was also confirmed by the increase in both ζ-potential and size due to the exposure of the polycation interlayer and the compromised colloidal stability. The silica interlayer rendered the SMA highly tolerant to dissociation induced by anionic lipids, while after 24 h dialysis siRNA release from the SMA was clearly observed, presumably due to gradual dissolution of the silica interlayer based on the equilibrium shift to silicate ions. The entrapment ratio of siRNA delivered by the SMA within the endosome was significantly lower than that by nondisulfide control (NDC) without PEG detachability, suggesting the improved endosomal escape of SMA with the exposed, endosome-disrupting interlayer after PEG detachment. SMAs induced significantly higher gene silencing efficiency in various cultured cells, compared to NDC, without associated cytotoxicity. The systemic administration of SMAs for subcutaneous tumor-bearing mice achieved significant endogenous gene silencing in tumor tissue without hematological toxicity.

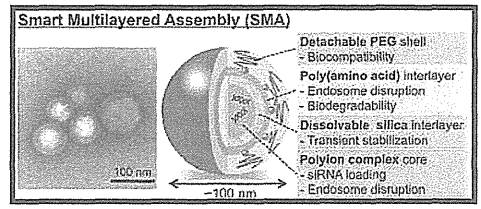

KEYWORDS: siRNA delivery · polyion complex · silica · poly(ethylene glycol) · layer-by-layer

Small interfering RNA (siRNA) has generated tremendous research interest in therapeutic applications for the treatment of various intractable diseases caused by aberrant gene expression, such as cancer.[1,2] This interest stems from the highly specific and potent gene silencing ability inherent to siRNA, termed RNA interference (RNAi). In order to attain therapeutic benefit, siRNA needs to overcome several biological hurdles, such as rapid renal clearance, enzymatic decomposition, distribution in nontarget tissues, inefficient cellular uptake, and endosomal/lysosomal entrapment. To date, various types of nanoparticle formulations have been developed as a delivery vehicle of siRNA, *e.g.*, polymer-based complexes (polyplexes),[3−12] lipid-based complexes (lipoplexes),[13−15] silica nanoparticles,[16,17] calcium phosphate nanoparticles,[18,19] gold nanoparticles,[20,21] and also their hybrid systems. Nevertheless, further improvement of siRNA vehicles is still demanded to gain better therapeutic efficacy for their translation into pharmaceutical agents.

Several properties required for the ideal siRNA vehicle are apparently conflicting, *i.e.*, high stability for siRNA protection in extracellular conditions *vs* smooth payload release within the cytoplasm and reduced nonspecific interactions with biomacromolecules (or biocompatibility) *vs* efficient cellular uptake (endocytosis) and subsequent endosomal escape in target cells. One promising solution to these conflicts is to design several smart materials, which exert the desired function in response to the specific biological environment, and then to integrate those component materials into one formulation toward multifunctionalities. For this purpose, construction of multilayered polyion complexes (PICs) by a layer-by-layer (LbL) technique allows the facile integration of a variety of charged components with different functionality as well as negatively charged nucleic acids into one nanoparticle.[22−24] A few recent

* Address correspondence to kataoka@bmw.t.u-tokyo.ac.jp, miyata@bmw.t.u-tokyo.ac.jp.

Received for review March 16, 2012 and accepted July 26, 2012.

Published online July 26, 2012
10.1021/nn301164a

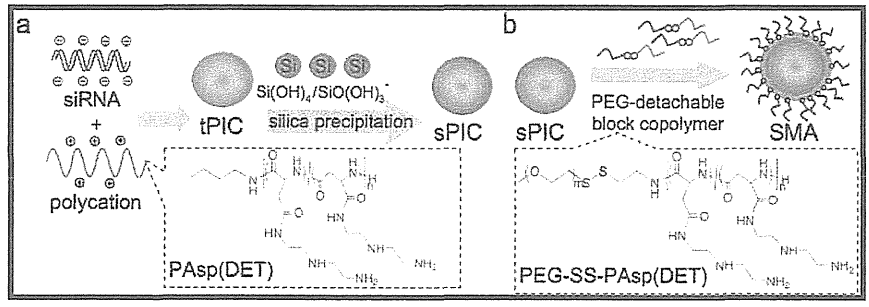

Figure 1. Preparation schemes of a smart multilayered assembly (SMA) by the layer-by-layer method. (a) Preparation of silica-coated PIC (sPIC) by silica-coating of the template PIC (tPIC). (b) Preparation of the SMA (PEG-SS-PAsp(DET)/silica-coated PAsp(DET)/siRNA PIC) by additional coating with PEG-block-polycation.

studies reported that the LbL technique successfully prepared siRNA-incorporating nano/microparticles from gold nanoparticle templates or mesoporous silica microparticle templates with several charged components for enhanced siRNA delivery.[25−27]

For transient stabilization of PIC structures, the covering of their surface with a silica layer is one of the promising approaches, because the silica layer (i) can be easily prepared on the surface of cationic PICs, (ii) is negatively charged, thus available as a substrate for additional adsorption of the oppositely charged components, and (iii) substantially stabilizes the PIC, while gradually dissolving for payload release under highly dilute conditions based on the equilibrium shift to silicate ions.[28,29] Indeed, our previous study revealed that the plasmid DNA-carrying PIC was successfully coated with a silica layer by simple incubation with sodium silicate solutions and was reversibly stabilized in a silicate concentration-dependent manner, leading to enhanced gene expression in cultured cells.[29] Meanwhile, for the preparation of biocompatible nanoparticles, installation of poly(ethylene glycol) (PEG) on their surface, termed PEGylation, is one of the most promising strategies. PEGylated nanoparticles are sterically stabilized by highly flexible and hydrated PEG chains, preventing the nanoparticles from secondary aggregate formation and nonspecific interactions with biomacromolecules, such as serum components and blood cells.[30−32] However, in the case of nucleic acid delivery, such PEG shielding has concurrently compromised the membrane-disrupting (or endosomal escape) functionality of nanoparticles, resulting in lower transfection efficiency (termed PEG dilemma).[33] To bypass this dilemma, several previous studies, including ours, demonstrated the utility of PEG-detachable systems, which are constructed by smart block copolymers of PEG and an endosome-disrupting polycation tethered by cleavable linkers in the endosome/lysosome, *e.g.*, a reductive environment-responsive disulfide bond[33,34] and an acidic pH-responsive hydrazone.[35] The PEG detachment within the endosome can expose the endosome-disrupting polycation on the nanoparticle surface for facilitated endosomal escape.

In the present study, a smart multilayered assembly (SMA) was developed with the PIC featuring a siRNA-loaded core, a transiently core-stabilizing silica interlayer, an endosome-disrupting polycation interlayer, and a detachable PEG shell, altogether aimed toward biocompatible and mutifunctional siRNA delivery (Figure 1). The distinctive feature of this formulation was that SMAs were constructed with soft materials, *i.e.*, hydrophilic polymers and nonannealed silica. They can be metabolized more rapidly in the body compared to previous formulations prepared from iron, gold, or annealed mesoporous silica nanoparticles, thereby providing a great advantage for multiple-dose administration. As the endosome-disrupting polycation, a polyaspartamide derivative bearing two repeating units of aminoethylene (termed PAsp(DET)) was selected and further tethered with PEG through a disulfide bond (−SS−), which can be cleaved by reducing enzymes on the cellular membrane or in the endosome/lysosome.[36,37] PAsp(DET) has been extensively shown to induce strong membrane disruption selectively at endosomal acidic pH (~5.5) for efficient, less toxic endosomal escape, probably due to the distinctive change in the protonated structure in the side chain, *i.e.*, the monoprotonated state at extracellular pH 7.4 and the diprotonated state at acidic pH.[38−42] The utility of SMAs was physicochemically and biologically investigated in comparison with the control without PEG detachability. In particular, the feasibility of SMAs for siRNA-based cancer therapy was examined with regard to endogenous gene silencing efficiency in a subcutaneous tumor model and also hematological toxicity after systemic administration. Ultimately, we demonstrate that SMAs may be promising formulations for successful siRNA delivery.

RESULTS AND DISCUSSION

Preparation and Physicochemical Characterization of the SMA. A SMA, that is, PEG-SS-PAsp(DET)/silica-coated PAsp(DET)/siRNA PIC, was prepared as illustrated in Figure 1. At first, the PAsp(DET)/siRNA-based template PIC (tPIC) was prepared by mixing siRNA with PAsp(DET) in a buffer solution (Figure 1a). A residual molar ratio of amines in PAsp(DET) to phosphate in siRNA = 3,

corresponding to a residual molar ratio of protonated amines in PAsp(DET) to phosphates in siRNA of 1.5,[12] was selected to obtain the positively charged tPIC with a minimal amount of unbound polycations for effective silica-coating. The formation of tPICs with a hydrodynamic size of 115 nm, a polydispersity index (PDI) of less than 0.1, and a positive ζ-potential (~20 mV) was confirmed with the Zetasizer (Table 1 and Figure 2a). It should be noted that PAsp(DET) was selected as a component polycation because of its considerably low cytotoxicity and excellent endosome-disrupting capability.[38−42] In detail, the protonation state of the side chain of PAsp(DET) changes from a monoprotonated state to a diprotonated state in response to the endosomal acidification. The membrane-disrupting activity of PAsp(DET) is quite low in the monoprotonated state, but is significantly augmented in the diprotonated state for effective endosome disruption. Despite the excellent endosome-disrupting capability of PAsp(DET), the low stability of PAsp(DET)/siRNA PICs in serum-containing media has substantially limited their gene silencing efficiency,[12,43,44] thereby requiring additional stabilization strategies for successful siRNA delivery.

According to the previously reported protocol,[29] silica-coating was performed by incubation of tPIC with sodium silicates in 10 mM HEPES buffer (pH 7.3) for 24 h at room temperature, then characterized with the Zetasizer. In the range of sodium silicate concentrations above 3 mM, the obtained PICs showed almost the same sizes (~130 nm) and negative ζ-potentials (~−20 mV) (Supporting Figure 2). Through incubation with silicates, the PIC size was considerably increased, and the ζ-potential was converted from the positive to the negative, well consistent with the formation of the anionic silica layer on the PIC surface. It should be noted that no leakage of siRNA from PICs was observed after silica-coating (Supporting Figure 3). The silica-coated PIC (sPIC) prepared at 3.5 mM sodium silicate was selected for the following experiments, as it exhibited the smallest size with relatively less silicates; at 3.5 mM sodium silicate sPICs had a hydrodynamic size of 125 nm, and a relatively narrow size distribution (PDI = 0.08) for a polymer-based self-assembly, a negative ζ-potential (−19 mV), and spherical morphology, as shown in dynamic light scattering (DLS) results (Table 1 and Figure 2a and b) and transmission electron microscopy (TEM) images (Figure 2d and Supporting Figure 5a).

Next, a smart polymer, PEG-SS-PAsp(DET), was utilized for the additional covering of sPIC for construction of the SMA (Figure 1b). Prior to addition of the polymer, the sPIC solution was applied to ultrafiltration (3000*g*, molecular weight cutoff: 300 000 Da) to remove the unbound silica species. Then, the purified sPIC solution was mixed with the polymer solution with varying concentrations, followed by 1 h incubation at room temperature. In the mixed solution, large aggregates (several μm in diameter) were formed in lower polymer concentrations (<250 μM in polymer amine) (Supporting Figure 4), probably due to the diminished electrostatic repulsion between the sPICs through charge neutralization of the surface silica by polymer binding. With further increase in polymer concentration, the PIC size was gradually decreased, presumably because of effective PEG-shielding, and consequently the size change leveled off at around a residual amino group concentration of 400 μM (equivalent to 5 times the siRNA phosphates in the solution). Considering the

TABLE 1. Size and Polydispersity Index (PDI) of PICs in 10 mM HEPES Buffer (pH 7.3), Determined by Dynamic Light Scattering

	diameter (nm)	PDI
tPIC	115 ± 8	0.08 ± 0.01
sPIC	125 ± 13	0.08 ± 0.01
SMA	159 ± 8	0.10 ± 0.03
NDC	159 ± 10	0.08 ± 0.03
NPC	143 ± 15	0.14 ± 0.04

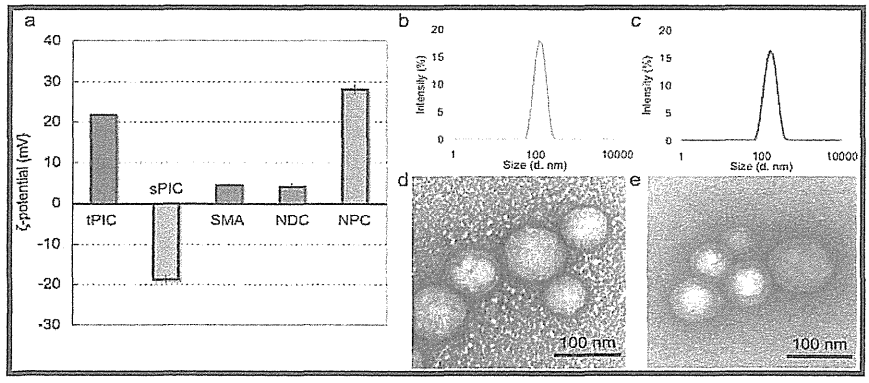

Figure 2. Physicochemical characterization of nanoparticle formulations. (a) ζ-Potential of PICs in 10 mM HEPES buffer (pH 7.3). (b, c) Intensity-based histograms of PICs determined by DLS: (b) sPIC and (c) SMA. (d, e) TEM images of PICs: (d) sPIC and (e) SMA (scale bar: 100 nm). PIC samples (2 μM siRNA) were applied onto a copper TEM grid with carbon-coated collodion film and stained with uranyl acetate solution (2% w/v).

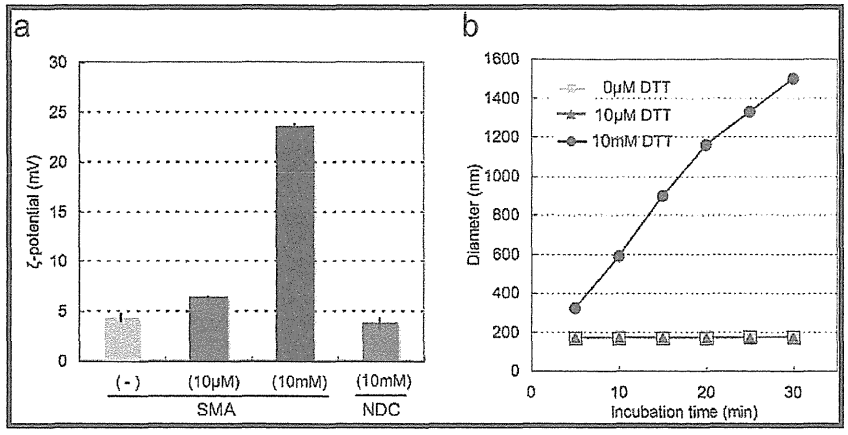

Figure 3. Reductive environment responsiveness of the SMA. (a) ζ-Potentials of the SMA and NDC after 30 min incubation in 10 mM HEPES buffer (pH 7.3) with or without DTT (0, 10 μM and 10 mM DTT). Results are expressed as mean and standard deviation (n = 3). (b) Time-dependent change in size of the SMA in 10 mM HEPES buffer containing 150 mM NaCl (solid squares); in 10 mM HEPES buffer containing 150 mM NaCl and 10 μM DTT (solid triangles); and in 10 mM HEPES buffer containing 150 mM NaCl and 10 mM DTT (solid circles), measured by DLS.

fact that an excess increase in polymer concentration may generate free (or uncomplexed) polymer in the solution, the sample prepared at a residual amino group concentration of 400 μM was selected for further studies.

The hydrodynamic size and ζ-potential of a series of siRNA PICs are summarized in Table 1 and Figure 2a. A non-PEGylated control (NPC), which was prepared by mixing sPIC with PAsp(DET) homopolymer, had a hydrodynamic size of 143 nm with a PDI of 0.14 and a strongly positive ζ-potential of 28 mV, suggesting the formation of a cationic PAsp(DET) outer layer. In contrast, the SMA as well as the nondisulfide control (NDC), which was prepared from PEG-PAsp(DET), had a hydrodynamic size of 159 nm with the PDI of ~0.10 and a ζ-potential close to neutral (~4 mV). The larger size ($P < 0.05$ for NPC) and the almost neutral ζ-potential of the SMA and NDC, compared with NPC, suggest that the sPIC should be successfully covered with a neutral PEG outer layer *via* the electrostatic interaction between anionic silica and the cationic PAsp(DET) segment of the block copolymers. Furthermore, the DLS and TEM histograms (Figure 2c and Supporting Figure 5b, respectively) and TEM images (Figure 2e and Supporting Figure 6) of the SMAs revealed that the relatively narrow size distribution and spherical morphology of sPICs were maintained. Note that the size distribution histograms obtained from TEM images were comparable to those from the number statistics of DLS (Supporting Figure 5).

Reductive Environment Responsiveness of the SMA. In order to examine the reductive environment-responsive PEG detachment from the SMA, the ζ-potential of the SMA was examined in 10 mM HEPES buffer (pH 7.3) containing different amounts of a reducing agent, dithiothreitol (DTT) (0, 10 μM and 10 mM). Note that 10 μM and 10 mM DTT were chosen to mimic the extracellular and the intracellular reducing potentials, respectively, generated by glutathione.[36] In 10 mM HEPES buffer (pH 7.3), the SMA was observed to have a ζ-potential close to neutral (~4 mV), suggesting the presence of a PEG shell that covers the nanoparticle. In contrast, after 30 min incubation in 10 mM HEPES buffer (pH 7.3) containing 10 mM DTT, the SMA exhibited an appreciably increased ζ-potential (24 mV), comparable to NPC, whereas a much lower ζ-potential was observed in the 10 μM DTT condition (Figure 3a). The appreciably increased ζ-potential of the SMA in the stronger reductive condition is well consistent with the exposure of the positively charged PAsp(DET) layer due to the PEG detachment based on the disulfide cleavage. The pivotal role of the disulfide bond for PEG detachment in the SMA is also suggested by the result that the NDC maintained the neutral ζ-potential even in the stronger reductive conditions (Figure 3a). The PEG detachability in the SMA was further examined from the standpoint of the colloidal stability of the nanoparticles. DLS measurement was conducted to monitor the size change of SMAs as well as NDCs and NPCs in 10 mM HEPES buffer (pH 7.3) containing 150 mM NaCl. First, the NDC and NPC were compared to estimate the effect of PEG on the size change. The size of the NPCs clearly increased over the incubation period, reaching μm dimensions in 30 min, presumably due to secondary aggregate formation under the physiological salt conditions, which attenuates the electrostatic repulsion between the charged nanoparticles (Supporting Figure 7). In contrast, this secondary aggregate formation was dramatically suppressed in the NDC formulation (Supporting Figure 7), demonstrating the enhanced colloidal stability of PICs with PEG palisades. Next, the SMAs were similarly evaluated by DLS in the same buffer with or without DTT (Figure 3b). At 0 and 10 μM DTT, no size change of the SMAs was observed following 30 min incubation, similar to NDCs, indicating that the colloidal stability of

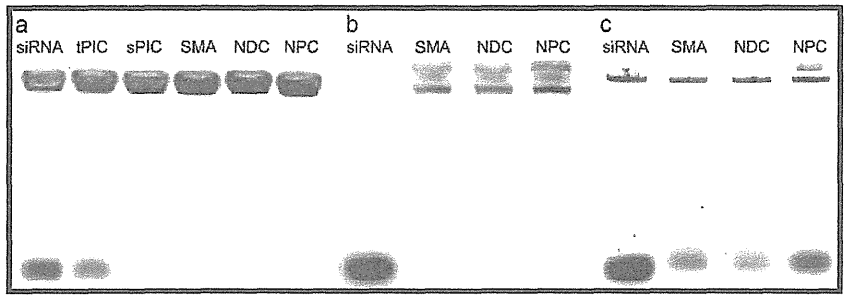

Figure 4. Tolerability of PICs against dissociation triggered by anionic lipids. siRNA release from PICs was evaluated by agarose gel electrophoresis. (a) Each PIC was incubated in 10 mM HEPES buffer (pH 7.3) containing anionic lipids, DOPS, for 48 h at a molar ratio of carboxyl groups in DOPS to phosphate groups in siRNA of 32. (b, c) Each PIC solution was dialyzed (molecular weight cutoff: 5000 Da) against a 1000-fold excess of 10 mM HEPES buffer (pH 7.3) for (b) 3 h and (c) 24 h. Then, each PIC solution was mixed with DOPS and incubated for 24 h, followed by electrophoresis.

the SMA was maintained even in mild reductive conditions. In sharp contrast, in the conditions containing 10 mM DTT, the increase in size of the SMA was clearly observed over the incubation period, similar to NPC (Supporting Figure 7), indicating the significantly compromised colloidal stability presumably due to the PEG detachment. Altogether, the PEG palisade in the SMA may sterically stabilize siRNA PICs in extracellular conditions, but can be removed on the cellular surface and/or in the endosome/lysosome with higher reducing potentials,[36,37] to expose the endosome-disrupting PAsp(DET) layer.

Stability Shift in the SMA with a Dissolvable Silica Interlayer. When administered in the body, siRNA PICs encounter abundant charged biomolecules, such as serum proteins and cell membranes, which may nonspecifically bind to the PICs, possibly leading to undesirable dissociation. Thus, high resistance toward such dissociation is a prerequisite for *in vivo* applications of siRNA PICs. In addition, once delivered into the cytoplasm, siRNA must also be released from PICs to allow association with RNAi-related proteins. Integration of a silica layer onto siRNA PICs should be a promising solution to overcome this conflicting requirement, because the silica layer stabilizes the siRNA PICs while also dissolving in a time-dependent manner in dilute conditions based on the equilibrium shift in the silicate ions.[29,45]

To investigate the stability shift induced by silica dissolution, the SMA was challenged by an anionic lipid, 1,2-dioleoyl-*sn*-glycero-3-phospho-L-serine sodium salt (DOPS),[46] before and after dialysis against a 1000-fold volume of 10 mM HEPES buffer (pH 7.3) for 3 and 24 h for removal of generated free silicates. Note that DOPS was selected as a model anionic molecule in this assay, as phosphatidylserine is one of the major components of cell membranes that can interact with siRNA PICs in intracellular conditions, thereby is useful for estimation of the feasibility of siRNA release from PICs in cells. Each sample was incubated with DOPS (the mixing ratio was set at a molar ratio of carboxyl groups in DOPS to phosphate groups in siRNA of 32), followed by agarose gel electrophoresis. As shown in Figure 4a, the band corresponding to naked siRNA was clearly observed for the tPIC sample incubated with DOPS, indicating PIC dissociation. In contrast, siRNA release was significantly suppressed for the SMA formulation as well as sPICs before dialysis. Thus, it was confirmed that the silica layer rendered siRNA PICs highly tolerant to counteranion-triggered dissociation. On the other hand, siRNA was considerably released from SMAs after dialysis for 24 h (Figure 4c), whereas release was still limited after dialysis for 3 h (Figure 4b). Note that a similar tendency was also observed for NDCs and NPCs featuring a silica layer (Figure 4a–c). These results demonstrate that the dissolvable silica layer in siRNA PICs can induce a stability shift for smooth release of siRNA in the cytoplasm.

Gene Silencing and Cell Viability Assays. The efficiency of gene silencing was evaluated using a luciferase assay against HuH7-Luc, a human hepatoma cell stably expressing luciferase. A linear polyethyleneimine-based transfection reagent (ExGen 500) was used as a positive control in this assay. As shown in Figure 5a, the SMA as well as NDC and NPC appreciably enhanced the gene silencing efficiency at higher siRNA concentrations, compared to tPIC and sPIC, suggesting that PAsp(DET)-based polymers bound onto a sPIC surface improved the siRNA delivery efficiency. Although there was no significant difference between SMAs and NDCs at the lowest siRNA concentration tested, the SMAs exerted significantly higher gene silencing efficiency than NDCs at higher siRNA concentrations ($P < 0.01$ at 200, 300, and 400 nM siRNA), suggesting that the enhanced efficiency of the SMA should be due to the PEG detachability. The exposure of the PAsp(DET) layer after the PEG detachment may improve the endosomal escape efficiency of siRNA PICs. On the other hand, the gene silencing efficiency of the SMAs was lower than that of NPCs as well as ExGen 500 (Figure 5a), probably due to more efficient cellular uptake of the non-PEGylated PICs, as shown in the next section. Despite lower gene silencing efficiency, the SMA formulation with PEG palisades is more suitable for systemic administration *in vivo*, because the much lower colloidal

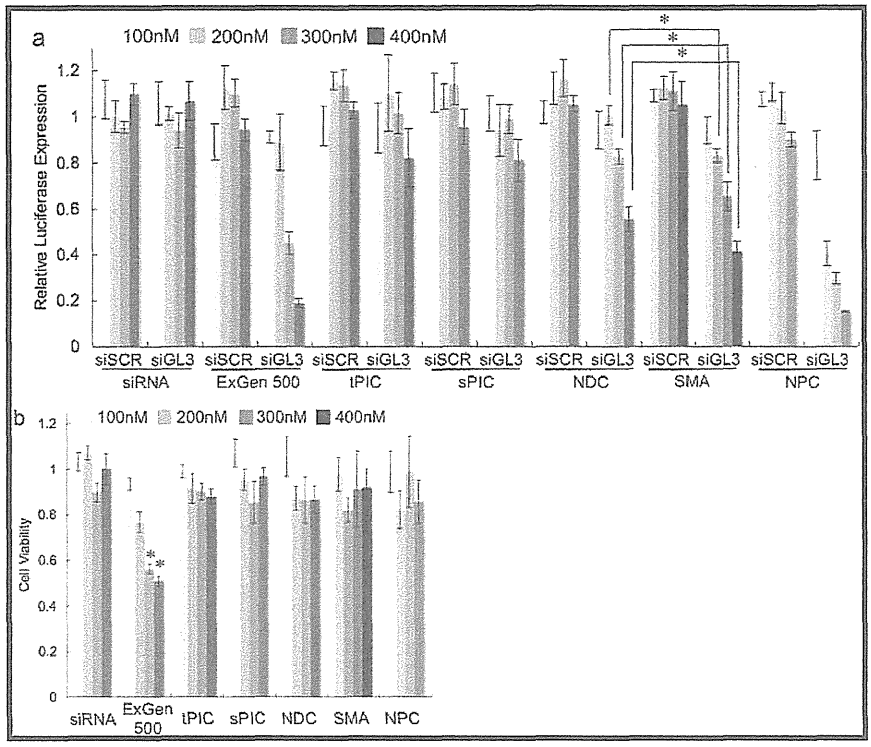

Figure 5. (a) Gene silencing activity against HuH7-Luc cells. Scramble siRNA (siSCR) was used as a control sequence for GL3 luciferase siRNA (siGL3). HuH7-Luc cells were treated with each PIC for 48 h (siRNA concentrations from the left: 100, 200, 300, and 400 nM) and subjected to the luciferase assay. Relative luciferase expression was calculated as the ratio of luciferase expression relative to nontreated cells. Results are expressed as mean and standard deviation ($n = 4$). *$P < 0.01$ for NDC. (b) Cell viability of HuH7-Luc cells in the same conditions as the gene silencing study was determined with the Cell Counting Kit-8 assay, with the cell viability of the nontreated cells set to 1. Results are expressed as mean and standard deviation ($n = 8$). *$P < 0.01$ compared to other samples. In both experiments, ExGen 500 was used according to the manufacturer's protocol as a commercially available positive control.

stability and strong positive ζ-potential of the non-PEGylated PICs would likely lead to the formation of secondary aggregates through nonspecific interactions with biomacromolecules during blood circulation.[32] Note that a similar profile in gene silencing efficiency was also observed in other luciferase-expressing cell lines, human lung cancer (A549-Luc) and human ovarian cancer (SKOV3-Luc) (Supporting Figure 8). Meanwhile, all the PAsp(DET)-based PICs (tPIC, sPIC, NDC, SMA, and NDC) did not show substantial toxicity in cultured cells, which was in sharp contrast to ExGen 500 (Figure 5b). Reduced cytotoxicity of PAsp(DET)-based formulations is consistent with the previous reports of nucleic acid delivery using PAsp(DET), which features a monoprotonated state in each side chain at an extracellular neutral pH with appreciably less cytoplasmic membrane damage compared to other polycations, such as polyethyleneimine.[12,40–42] Thus, the SMA is demonstrated to enhance the siRNA delivery efficiency without increasing the cytotoxicity.

Cellular Uptake and Intracellular Distribution Studies. The mechanism of the enhanced gene silencing achieved by the SMA was further investigated in comparison with the controls (NDC and NPC as well as sPIC). To quantify the cellular uptake of each siRNA PIC by HuH7-Luc cells, the cells were incubated with the PICs prepared from Cy3-labeled siRNA (Cy3-siRNA) for 24 h and then subjected to flow cytometric analysis. As shown in Figure 6, the cellular uptake of Cy3-siRNA PICs was increased in the polymer/silica-coated systems (SMA, NDC, and NPC), compared to sPIC. In detail, the Cy3-siRNA uptake of the SMA was significantly higher than that of sPIC ($P < 0.05$) and significantly less than that of NPC ($P < 0.01$), whereas no statistical difference was observed between PEGylated systems (SMA and NDC) ($P > 0.05$). The observed cellular uptake profile was apparently correlated with the surface charge of PICs; higher fluorescence (or cellular uptake) was obtained by the PICs showing a higher ζ-potential (Figure 2a), possibly due to the fact that the positively charged surface should facilitate an association with the anionic cytoplasmic membrane.[47,48] It should be noted that NPCs are likely to form secondary aggregates in the cell culture medium due to their lower colloidal stability (Supporting Figure 7), possibly affecting the cellular association and uptake. The significantly limited uptake efficiency observed for the SMA, compared to NPC, suggests that the PEG shell in the SMA might be effectively maintained during

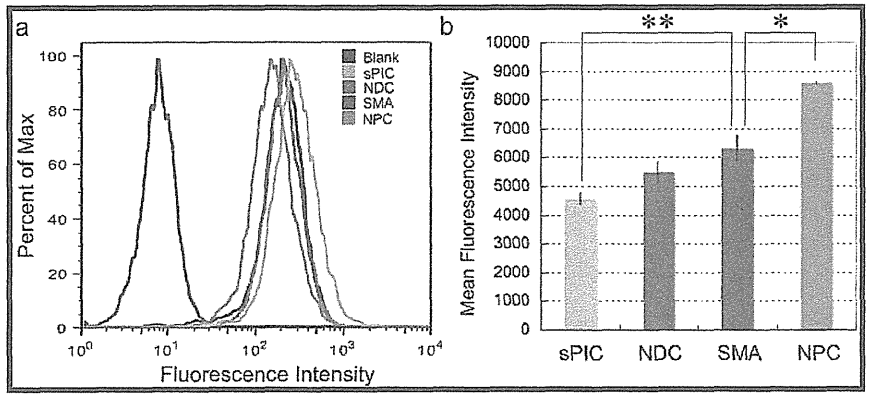

Figure 6. Cellular uptake of Cy3-siRNA PICs evaluated by flow cytometric analysis. HuH7-Luc cells were incubated with each PIC (siRNA concentration: 400 nM) for 24 h. (a) Flow cytometric data shown in the histogram. (b) Flow cytometric data shown in the bar graph. Results are expressed as mean and standard deviation ($n = 3$). *$P < 0.01$ for NPC. **$P < 0.05$ for sPIC.

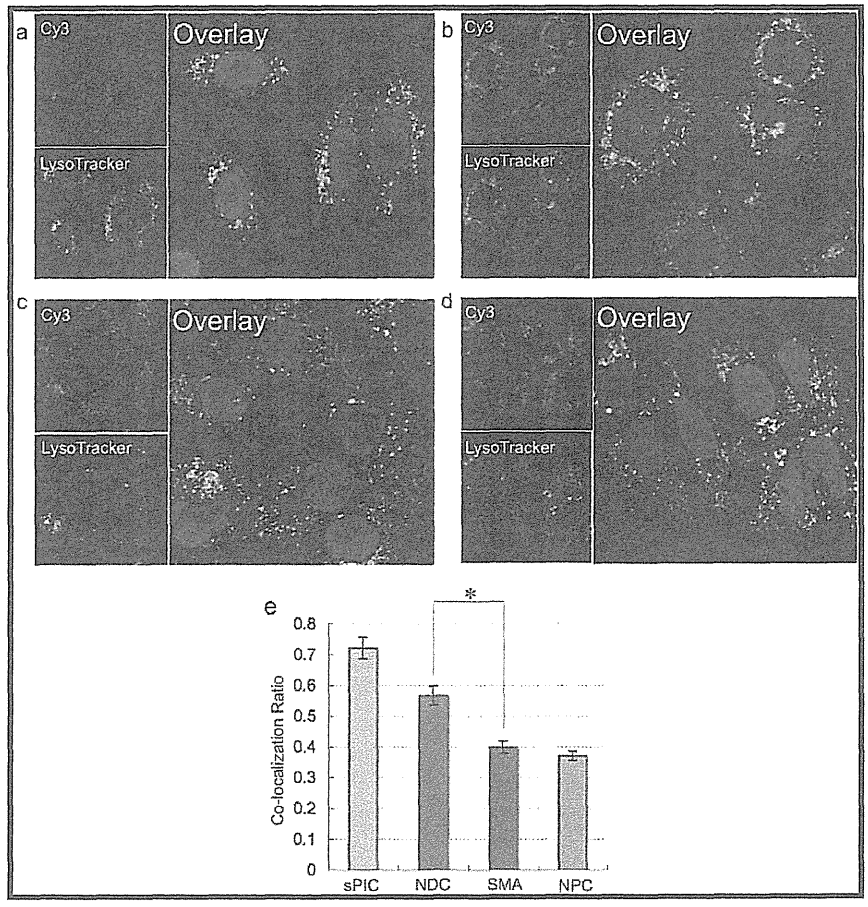

Figure 7. Intracellular distribution of Cy3-siRNA PICs. (a–d) CLSM images of (a) sPIC, (b) NDC, (c) SMA, and (d) NPC (red: Cy3-siRNA, green: LysoTracker Green, blue: Hoechst33342). HuH7-Luc cells were incubated with each PIC at 400 nM siRNA for 24 h. (e) Co-localization ratio of Cy3-siRNA with the late endosome/lysosome marker (LysoTracker Green) calculated from the number of pixels in the obtained CLSM images. Results are expressed as mean and standard deviation ($n = 20$). *$P < 0.01$ for NDC.

incubation in the cell culture medium. The facilitated cellular uptake in the polymer/silica-coated systems, especially in NPC, might contribute to their enhanced gene silencing efficiency (Figure 5a). Nevertheless, the similar uptake efficiency between the SMA and NDC also suggests that there is another crucial factor to explain their significantly different gene silencing efficiency (Figure 5a), as demonstrated by the following confocal laser scanning microscopic (CLSM) analysis.

Once endocytosed by cells, siRNA PICs were generally transported to the late endosome/lysosome, which is the digestive organelle. Thus, the efficient

endosomal escape of PICs is critical for successful siRNA delivery into the cytoplasm. Herein, the intracellular distribution of Cy3-siRNA PICs was observed using CLSM after 24 h incubation with the cells. In the obtained CLSM images, the signals from Cy3-siRNA, LysoTracker Green, and Hoechst33342 are shown in red, green, and blue, respectively (Figure 7a–d). The endosomal entrapment efficiency was further estimated by calculating the number ratio of the pixels of Cy3-siRNA co-localizing with the late endosome/lysosome marker (yellow) to all the pixels of Cy3-siRNA (yellow and red). Obviously, the co-localization ratios in the polymer/silica-coated systems (SMA, NDC, and NPC) were lower than that in sPIC (Figure 7e), indicating that efficient endosomal escape should be induced by the coating of sPIC with PAsp(DET)-based polymers. Notably, the SMA featuring the detachable PEG shell showed a significantly lower co-localization ratio than NDC ($P < 0.01$), suggesting that reductive environment-responsive PEG detachment (Figure 3) might accelerate the endosomal escape of the SMA for the significantly enhanced gene silencing efficiency (Figure 5a).

Therapeutic Gene Silencing *in Vitro* and *in Vivo*. To further examine the potential utility of the SMA formulation for siRNA-based cancer therapy, the gene silencing ability of SMAs was investigated *in vitro* and *in vivo* for a therapeutic gene targeting the human renal cancer cell line OS-RC-2. Treatment of renal cancer with siRNA is a particularly attractive therapeutic target, as highly effective clinical anticancer drugs are currently unavailable. Vascular endothelial growth factor (VEGF) was selected as the target gene, because VEGF is a proangiogenic molecule that is overexpressed in a wide variety of cancer cells to stimulate angiogenesis and tumor growth.[49] To date, several previous studies demonstrated that VEGF gene silencing in tumor tissues significantly inhibits tumor growth.[34,50–53] Thus, the gene silencing ability of SMAs containing siRNA targeted toward VEGF (siVEGF) was examined in cultured OS-RC-2 cells by real-time reverse transcriptional PCR (RT-PCR). As shown in Figure 8a, SMAs containing siVEGF significantly reduced the VEGF mRNA level (~57%), compared to control SMAs containing scramble siRNA (siSCR).

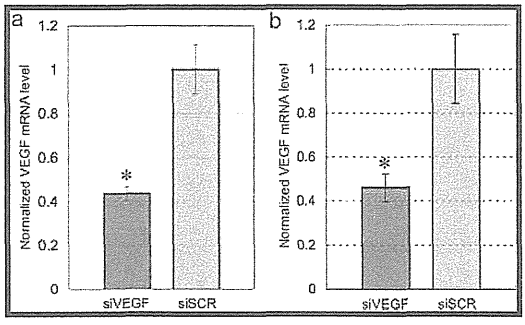

Figure 8. (a) *In vitro* VEGF gene silencing activity of SMAs in OS-RC-2 cells determined by RT-PCR. OS-RC-2 cells were incubated with SMAs for 48 h (siRNA concentration: 200 nM) prior to RT-PCR analysis. (b) *In vivo* VEGF gene silencing activity of SMAs in subcutaneous OS-RC-2 tumors. SMAs were intravenously injected into mice (1.25 mg siRNA/kg mouse) at days 1 and 2, and at day 3 subcutaneous tumors were excised and total RNA was extracted. In both *in vitro* and *in vivo* experiments, the level of VEGF mRNA was normalized to actin mRNA, and scramble siRNA (siSCR) was used as a control sequence for VEGF siRNA (siVEGF). Results are expressed as mean and standard error of the mean ($n = 4$). *$P < 0.05$ compared to siSCR.

Next, the *in vivo* gene silencing activity of siRNA delivered in SMAs was investigated using a subcutaneous OS-RC-2 tumor model following systemic administration by tail vein injection (1.25 mg siRNA/kg mouse). Prior to the gene silencing assay, several hematological parameters of mice treated with SMAs containing siSCR were monitored 24 h after systemic administration as indices of *in vivo* toxicity. Analysis of hematological parameters revealed that systemically administered SMA induced no problematic hematological toxicity (Table 2). For *in vivo* gene silencing assays, each mouse was injected twice at days 1 and 2, and at day 3 subcutaneous tumors were excised and RNA was extracted for RT-PCR. Figure 8b clearly shows that systemic administration of SMAs containing siVEGF induced significant reduction in the VEGF mRNA level (~50%) in the tumor tissue, compared to the control containing siSCR ($P < 0.05$), demonstrating the sequence-specific gene silencing ability of siRNA delivered by SMAs. Altogether, these results demonstrate the strong potential of SMAs for systemic siRNA delivery to tumor tissues without adverse side effects.

CONCLUSIONS

In this study, a smart multilayered assembly was prepared by a layer-by-layer method with PICs to feature a siRNA-loaded core, a transiently core-stabilizing silica interlayer, an endosome-disrupting PAsp(DET) interlayer, and a detachable PEG shell for

TABLE 2. Hematological Parameters of Mice Treated with SMA[a]

	siRNA dose (mg/kg)	ALT (U/L)	AST (U/L)	RBC ($\times 10^5/\mu L$)	WBC ($\times 10^2/\mu L$)	hemoglobin (g/dL)
buffer control	0	48 ± 4	54 ± 2	100 ± 2	27 ± 4	14.4 ± 0.3
SMA	1.25	43 ± 5	49 ± 4	97 ± 4	30 ± 4	14.4 ± 0.5

[a] Blood samples ($n = 4$) were collected 24 h after systemic administration. ALT: alanine aminotransferase; AST, aspartate aminotransferase; RBC, red blood cells; WBC, white blood cells.

multifunctional siRNA delivery. The successful preparation was confirmed by the change in size and ζ-potential of the PICs as well as their TEM images. The PEG detachability of the SMA in response to the reductive conditions was also confirmed by the change in size (or colloidal stability) and ζ-potential. The silica interlayer in the SMA substantially improved the tolerability of siRNA PICs to the dissociation triggered by the anionic lipids, while significant siRNA release was induced after the dialysis for removal of generated free silicates, indicating the dissolvable nature of the silica interlayer. SMAs significantly enhanced gene silencing for not only a reporter gene but also an endogenous therapeutic gene (VEGF) in cultured cancer cells without increased cytotoxicity. The major mechanism for the enhanced gene silencing in SMA was probably the facilitated endosomal escape of siRNA PICs through endosome disruption by the exposed PAsp(DET) layer after PEG detachment. Ultimately, systemic administration of SMAs into subcutaneous tumor-bearing mice resulted in significant VEGF gene silencing in the tumor tissue without problematic hematological toxicity. These results demonstrate the potential utility of the SMA formulation for systemic siRNA delivery aimed toward cancer therapy.

MATERIALS AND METHODS

Materials. α-Methoxy-ω-mercapto poly(ethylene glycol) (PEG-SH, M_n = 10 000) and α-methoxy-ω-amino poly(ethylene glycol) (PEG-NH_2, M_n = 12 000) were obtained from NOF Co. (Tokyo, Japan). β-Benzyl L-aspartate *N*-carboxy anhydride (BLA-NCA) was purchased from Chuo Kaseihin Co., Inc. (Tokyo, Japan). Methanol (MeOH), 2-aminoethanethiol, benzene, hexane, ethyl acetate, *N*,*N*-dimethylformamide (DMF), dichloromethane (DCM), diethylenetriamine (DET), *N*-methyl-2-pyrrolidone (NMP), *n*-butylamine, and dithiothreitol (DTT) were purchased from Wako Pure Chemical Industries, Ltd. (Osaka, Japan). DMF, DCM, NMP, *n*-butylamine, and DET were distilled before use. Dulbecco's modified Eagle's medium (DMEM) was purchased from Sigma Aldrich (St. Louis, MO, USA). Fetal bovine serum (FBS) was purchased from Dainippon Sumitomo Pharma Co, Ltd. (Osaka, Japan). Sterile HEPES (1 M, pH 7.3) was purchased from Amresco (Solon, OH, USA). The luciferase assay system was purchased from Promega Co. (Madison, WI, USA). All the RNA molecules, including 5′-Cy3-labeled RNA, were synthesized by Hokkaido System Science (Hokkaido, Japan). The sequences are as follows: GL3 luciferase siRNA (sense: 5′-(Cy3-)CUU ACG CUG AGU ACU UCG AdTdT-3′, antisense: 5′-UCG AAG UAC UCA GCG UAA GdTdT-3′), human VEGF siRNA (sense: 5′-GAU CUC AUC AGG GUA CUC CdTdT-3′, antisense: 5′-GGA GUA CCC UGA UGA GAU CdTdT-3′), and scramble siRNA (sense: 5′-UUC UCC GAA CGU GUC ACG UdTdT-3′, antisense: 5′-ACG UGA CAC GUU CGG AGA AdTdT-3′).

Synthesis of PEG-SS-NH_2. α-Methoxy-ω-dithioamino poly(ethylene glycol) (PEG-SS-NH_2) was synthesized as previously described.[33] In brief, PEG-SH (3.75 g, 0.375 mmol) was dissolved in methanol (400 mL) containing 28% sodium methoxide. 2-Aminoethanethiol (4.23 g, 37.3 mmol) was added to the PEG-SH solution, and the mixture was stirred for 5 days at room temperature. Then, the reaction solution was neutralized with cold 5 N HCl (8.15 mL, 40.8 mmol), followed by dialysis against distilled water for 1 day. The dialyzed solution was further purified through the ion-exchange resin (SP-Sephadex C-50, solute: H_2O), followed by lyophilization to obtain PEG-SS-NH_2 as a chloride salt form. Finally, PEG-SS-NH_3Cl dissolved in deionized water was dialyzed against 0.1% NH_3 solution for 1 day to deprotonate the amino group of the PEG-SS-NH_2. Then, the sample (PEG-SS-NH_2) was lyophilized and collected (2.76 g, 0.276 mmol).

Synthesis of PEG-SS-PBLA, PEG-PBLA, and PBLA. Poly(ethylene glycol)-disulfide-poly(β-benzyl L-aspartate) (PEG-SS-PBLA), poly(ethylene glycol)-poly(β-benzyl L-aspartate) (PEG-PBLA), and poly(β-benzyl L-aspartate) (PBLA) were synthesized by the ring-opening polymerization of BLA-NCA initiated by PEG-SS-NH_2, PEG-NH_2, and *n*-butylamine, respectively, according to the previously described method.[33] The typical synthetic procedure is briefly shown for PEG-SS-PBLA. PEG-SS-NH_2 (0.40 g, 0.04 mmol) and BLA-NCA (1.08 g, 4.32 mmol) were dissolved in DCM (6.0 mL) and DMF (1.5 mL), respectively. The solution containing BLA-NCA was added to the PEG-SS-NH_2 solution and stirred at 35 °C under an argon atmosphere. After 48 h, the reaction solution was precipitated in hexane/ethyl acetate (6:4 v/v) and dried overnight under reduced pressure to obtain PEG-SS-PBLA (1.12 g, yield 87%). In order to determine the molecular weight distribution (M_w/M_n) of the obtained polymer, size exclusion chromatography (SEC) was performed using a TOSOH HLC-8820 equipped with TSK gel columns (SuperAW4000 and SuperAW3000 × 2, TOSOH, Japan) and an internal refractive index detector at a flow rate of 0.3 mL min^{-1} at 40 °C. NMP with 10 mM LiBr was used as an eluent. A narrow M_w/M_n (= 1.10) was confirmed from the SEC (data not shown). PEG-PBLA and PBLA were synthesized in a similar manner; *e.g.*, BLA-NCA (840 mg, 3.36 mmol) and PEG-NH_2 (370 mg, 0.03 mmol) for PEG-PBLA (926 mg, yield 93%); and BLA-NCA (1.40 g, 4.86 mmol or 1.21 mg, 4.20 mmol) and *n*-butylamine (6.00 mL, 0.0607 mmol or 2.93 μL, 0.0296 mmol) for PBLA with different degrees of polymerization (DPs) (888 mg, yield 77% or 910 mg, yield 91%), respectively. The DPs of the PBLA segment in PEG-SS-PBLA and PEG-PBLA were calculated to be 87 and 92, respectively, from the peak intensity ratio of the PEG protons to the benzyl protons ($C_6H_5CH_2-$, δ = 5.1 and 7.3 ppm) at the side chain, and the DPs of two PBLAs were determined to be 92 and 225 from the peak intensity ratio of the butyl protons ($CH_3CH_2CH_2CH_2-$, δ = 0.8–1.5 ppm) at the α-chain end to the benzyl protons ($C_6H_5CH_2-$, δ = 5.1 and 7.3 ppm) at the side chain in the ^{1}H NMR spectrum (polymer concentration: 10 mg/mL, solvent: dimethyl sulfoxide-d_6, temperature: 80 °C) (data not shown).

Synthesis of PEG-SS-PAsp(DET), PEG-PAsp(DET), and PAsp(DET). Introduction of a *N*′-[*N*-(2-aminoethyl)-2-aminoethyl] moiety into the polyaspartamide side chain was performed by the aminolysis reaction of benzyl groups of the PBLA segment with DET as previously described.[33] Briefly, a typical synthetic procedure is shown for poly(ethylene glycol)-disulfide-poly{*N*′-[*N*-(2-aminoethyl)-2-aminoethyl]aspartamide} (PEG-SS-PAsp(DET)). PEG-SS-PBLA (200 mg, 7 μmol) lyophilized from a mixed solution of DCM (5 mL) and benzene (20 mL) was dissolved in NMP (10 mL) under an argon atmosphere. DET (3.44 mL, 32 mmol, 50 equiv to benzyl group in PEG-SS-PBLA) was dissolved in NMP (3.44 mL). The PEG-SS-PBLA solution was then added to the cooled DET solution and stirred at 4 °C for 1 h under an argon atmosphere. The reaction solution was added dropwise into cold 5 N HCl_{aq} (19.2 mL, 96 mmol) for neutralization and subsequently dialyzed against 0.01 M HCl_{aq} for 24 h and deionized water for an additional 24 h using a dialysis membrane (molecular weight cutoff: 6000–8000 Da). The dialyzed solution was lyophilized to obtain PEG-SS-PAsp(DET) as a hydrochloride salt (170 mg, yield 70%). Poly(ethylene glycol)-poly{*N*′-[*N*-(2-aminoethyl)-2-aminoethyl]aspartamide} (PEG-PAsp(DET)) and poly{*N*′-[*N*-(2-aminoethyl)-2-aminoethyl]aspartamide} (PAsp(DET)) were synthesized in a similar manner, *e.g.*, PEG-PBLA (103 mg, 3.20 μmol) and DET (1.5 mL, 14.7 mmol) for PEG-PAsp(DET) (98.0 mg, yield 85%); and PBLA (149 mg, 7.90 μmol)

and DET (3.9 mL, 38.2 mmol) for PAsp(DET) (182 mg, yield 91%). The quantitative conversion of PBLA to PAsp(DET) in PEG-SS-PAsp(DET) and PEG-PAsp(DET) was confirmed from the peak intensity ratio of the protons of the PEG chain ($-(CH_2)_2$-O-, δ = 3.7 ppm) to those of the ethylene unit in the 1,2-diaminoethane ($H_2N(CH_2)_2NH(CH_2)_2NH-$, δ = 3.1–3.5 ppm) moieties in the side chain of PAsp(DET) in the ^{1}H NMR spectra (polymer concentration: 10 mg/mL, solvent: D_2O, temperature: 80 °C) (Supporting Figure 1a and b, respectively). In the case of PAsp(DET), the quantitative conversion was confirmed from the peak intensity ratio of the protons of the butyl group at the α-chain end ($CH_3CH_2CH_2CH_2-$, δ = 0.8–1.5 ppm) to the ethylene protons in the 1,2-diaminoethane ($H_2N(CH_2)_2NH(CH_2)_2NH-$, δ = 3.1–3.5 ppm) moieties in the side chain of PAsp(DET) in the ^{1}H NMR spectra (polymer concentration: 10 mg/mL, solvent: D_2O, temperature: 80 °C) (Supporting Figure 1c and d).

Preparation of a Series of PICs. PAsp(DET) (DP = 225) was dissolved in 10 mM HEPES buffer (pH 7.3) at a concentration of 5 mg/mL. Then, the PAsp(DET) solution was mixed with 15 μM siRNA (10 mM HEPES buffer, pH 7.3) to obtain an siRNA-incorporating PIC (final siRNA concentration: 2 μM). The residual molar ratio of amines in PAsp(DET) to phosphates in siRNA in the PIC solution was set to 3 to obtain a slightly positive PIC without an excess amount of polycations. After 30 min incubation at 4 °C, varying concentrations of sodium silicate solutions (10 mM HEPES buffer (pH 7.3)) were added to the PIC solution (final siRNA concentration: 1 μM). After 24 h incubation at room temperature, the mixed solution was purified by ultrafiltration (3000*g*, molecular weight cutoff: 300,000 Da) to remove the unbound silica species. Then, the purified solutions were mixed with the solution containing PEG-SS-PAsp(DET), PEG-PAsp(DET), or PAsp(DET) (DP = 92) (final siRNA concentration: 2 μM), followed by incubation at 25 °C for 1 h to obtain polymer/silica-coated PICs.

Size and ζ-Potential Measurements. The size and ζ-potential of each PIC were measured using a Zetasizer Nano-ZS instrument (Malvern Instruments, Malvern, UK) equipped with a He–Ne ion laser (λ = 633 nm) as an incident beam at a detection angle of 173° and at a temperature of 25 °C. In DLS, each PIC solution (20 μL, 1 μM siRNA, 10 mM HEPES buffer (pH 7.3) with or without 150 mM NaCl) was added into a low-volume cuvette (Malvern Instruments, Malvern, UK) for the measurements. The cumulant method was used to analyze the data obtained from the decay in the photon correlation function to obtain the hydrodynamic diameters and polydispersity indices. The results were shown as mean and standard deviation of the mean obtained from eight samples.

For ζ-potential measurement, each sample (700 μL, 1 μM siRNA, 10 mM HEPES buffer (pH 7.3)) was put into a folded capillary cell (Malvern Instruments, Malvern, UK). The obtained electrophoretic mobility was converted to the ζ-potential by applying the Smoluchowski equation: $\zeta = 4\pi\eta\nu/\varepsilon$ (η: viscosity of the solvent, ν: electrophoretic mobility, ε: dielectric constant of the solvent). The results were shown as mean and standard deviation obtained from three samples.

Transmission Electron Microscopic Observation. TEM observation was conducted using an H-7000 electron microscope (Hitachi, Tokyo, Japan) operated at 75 kV acceleration voltage. Copper TEM grids with carbon-coated collodion film were glow-discharged for 10 s using an Eiko IB-3 ion coater (Eiko Engineering Co. Ltd., Japan). The grids were dipped into PIC solution (2 μM siRNA), which was mixed with uranyl acetate solution (2% w/v) for 60 s. After removal of excess solution with a filter paper, the sample grids were allowed to dry in air and then TEM observation was performed.

Agarose Gel Electrophoresis. siRNA release from PICs caused by an anionic lipid, 1,2-dioleoyl-*sn*-glycero-3-phospho-L-serine sodium salt, was evaluated by agarose gel electrophoresis for estimation of the PIC stability. Each PIC solution (2 μM siRNA) was mixed with DOPS solution (2 mg/mL) at a molar ratio of carboxyl groups in DOPS to phosphate groups in siRNA of 32. After 48 h incubation at room temperature, the mixed solutions were subjected to electrophoresis by 0.9 wt % agarose gel in the TAE buffer (pH 7.4). siRNA in the gel was stained by ethidium bromide and analyzed by an FX molecular imager (BIO-RAD) equipped with Quantity One software (BIO-RAD).

Gene Silencing Assay. The gene silencing efficiency of the PICs was evaluated from the luciferase-based luminescence intensity of luciferase-expressing human hepatoma cells, HuH7-Luc. The cells were plated on a 48-well plate at a cell density of 5000 cells/well in DMEM supplemented with 10% FBS and incubated for 24 h. Then, the old medium was replaced with fresh medium, and PICs were added at a concentration of 100, 200, 300, and 400 nM siRNA. After 48 h incubation, the PIC-containing medium was removed. After washing with 100 μL of PBS, the cells were lysed with 100 μL of the cell culture lysis buffer (Promega). The luciferase expression in the lysate was measured using a luciferase assay system (Promega) and a luminescence microplate reader (Mithras LB 940, Berthold Technologies, Bad Wildbad, Germany). The relative luciferase expression of the cells treated with PICs was calculated as a ratio of the expression of nontreated cells. The results were expressed as mean and standard deviation obtained from four samples.

Cell Viability Assay. HuH7-Luc cells were plated on a 48-well plate at a cell density of 5000 cell/well in DMEM supplemented with 10% FBS. After incubation for 24 h, the old medium was replaced with fresh medium, and the PICs were applied at a concentration of 100, 200, 300, and 400 nM siRNA. After 48 h incubation, the cell viability assay was performed using Cell Counting Kit-8 with WST-8, a soluble tetrasolium salt, according to the manufacturer's protocol (Dojindo, Japan). The absorbance was measured using a microplate reader with a filter of 450 nm (model 680, BIO-RAD). The cell viability was determined as a percentage of the absorbance of nontreated cells. The results were expressed as mean and standard deviation obtained from eight samples.

Flow Cytometric Analysis. HuH7-Luc cells were plated on a 12-well plate at a cell density of 25 000 cells/well in DMEM supplemented with 10% FBS and incubated for 24 h. The PICs prepared from Cy3-siRNA were applied to each well at a concentration of 400 nM siRNA. After 24 h incubation, cells were washed three times with PBS, treated with a trypsin-EDTA solution, and suspended in PBS. The fluorescence intensity of the suspended solutions was measured using a BD LSR II flow cytometer (BD Biosciences). The results were expressed as mean and standard deviation obtained from three samples.

Confocal Laser Scanning Microscopic Observation. HuH7-Luc cells were plated on a 35 mm glass-based dish (Iwaki, Tokyo, Japan) at a density of 50 000 cells/well in DMEM supplemented with 10% FBS and incubated for 24 h. The old medium was replaced with fresh medium, and each sample prepared from Cy3-siRNA was applied at 400 nM siRNA. After 24 h treatment with PICs, the transfection medium was removed and then staining with LysoTracker Green (Molecular Probes, Eugene, OR, USA) and Hoechst 33342 (Dojindo, Japan) in the medium was performed. The CLSM imaging was conducted using a LSM 510 (Carl Zeiss, Oberlochen, Germany) equipped with a C-Apochromat 63× objective (Carl Zeiss). The LysoTracker Green, Cy3-siRNA, and Hoechst 33342 were excited at 488 nm (Ar laser), 543 nm (He–Ne laser), and 710 nm (MaiTai laser for two-photon imaging), respectively.

The intracellular distribution of Cy3-siRNA was quantitatively evaluated by calculating the co-localization ratio of Cy3-siRNA pixels with LysoTracker Green pixels.[12,42] The calculation was conducted as follows:

$$\text{Co-localization ratio (\%)} = 100 \times \text{number of yellow pixels} / \text{number of yellow and red pixels}$$

The results are expressed as mean and standard deviation obtained from 20 cells.

RNA Recovery from Cultured and Subcutaneous OS-RC-2. Endogenous gene silencing efficiency of SMAs was evaluated using a human renal cell carcinoma, OS-RC-2 (RIKEN Bioresource Center, Tsukuba, Japan). For *in vitro* experiments, the cells were seeded onto a 12-well plate at a cell density of 125 000 cells/well in RPMI-1640 containing 10% FBS. After 24 h incubation, the medium was exchanged, and SMAs containing siVEGF or siSCR

were added at 200 nM siRNA. After 48 h incubation, the cells were lysed in 1 mL of Isogen (Nippon Gene, Tokyo, Japan), followed by RNA extraction by a conventional method with chloroform and 2-propanol. For *in vivo* experiments, Balb/c nude mice (male, 6-weeks-old) were subcutaneously inoculated with OS-RC-2 cells (10^7 cells/mouse), and tumors were allowed to grow for 1 week before sample injection. SMAs prepared at 2 μM siVEGF or siSCR were concentrated to 10 μM siRNA using a Vivaspin column (Sartorius Stedim Biotech, Bohemia, NY, USA) and then injected *via* the tail vein two times at days 1 and 2 (25 μg of siRNA in 200 μL per injection). At day 3, each tumor was excised and lysed in 0.5 mL of Isogen with sonication, followed by RNA extraction.

Real-Time RT-PCR. After RNA extraction, the RNA concentration in each sample was adjusted to ~20 μg/mL. Genomic DNA elimination and cDNA synthesis were performed using a ReverTra Ace qPCR RT Master Mix with gDNA Remover (Toyobo, Osaka, Japan) according to the manufacturer's protocol. Real-time RT-PCR was performed using an ABI 7500 Fast real-time RT-PCR system (Applied Biosystems, Foster City, CA, USA) with QuantiTect SYBR Green PCR Master Mix (Qiagen, Valecia, CA, USA). Human actin was used as a housekeeper gene (internal standard), and obtained data were normalized before statistical analysis. VEGF primer (forward: AGTGGTCCCAGGCTGCAC, reverse: TCCATGAACTTCACCACTTCGT) and actin primer (forward: CCAACCGCGAGAAGATGA, reverse: CCAGAGGCGTACAGGGATAG) used for RT-PCR were obtained from Hokkaido System Science (Hokkaido, Japan). The results were expressed as mean and standard error of the mean from four samples.

Hematological Toxicity Assay. SMAs were intravenously injected into the tail vein of Balb/c mice (male, 7-weeks-old), similar to the *in vivo* gene silencing assay (25 μg of siRNA in 200 μL per injection). HEPES buffer (10 mM, pH 7.4) containing 150 mM NaCl was used as a control solution. After 24 h, the mice were anesthetized and their blood was collected from the postcaval vein. The collected blood was analyzed to determine the level of ALT and AST with DRI-CHEM 7000i (Fuji Film, Tokyo, Japan) and the level of RBC, WBC, and hemoglobin with pocH-100iV Diff (Sysmex, Hyogo, Japan) according to the manufacturer's protocol. The results were expressed as mean and standard error of the mean from four samples.

Data Analysis. The experimental data were analyzed by Student's *t*-test. $P < 0.05$ was considered statistically significant.

Conflict of Interest: The authors declare no competing financial interest.

Acknowledgment. This research was financially supported by the Funding Program for World-Leading Innovative R&D on Science and Technology (FIRST) from the Japan Society for the Promotion of Science (JSPS) and also by Izumi Science and Technology Foundation. Part of this work was conducted in the Research Hub for Advanced Nano Characterization, The University of Tokyo, supported by the Ministry of Education, Culture, Sports, Science and Technology (MEXT), Japan. We are grateful to Dr. S. Fukuda (The University of Tokyo) and Mr. H. Hoshi (JEOL Ltd.) for their help with TEM observation.

Supporting Information Available: ^{1}H NMR spectra of PEG-SS-PAsp(DET) (Figure 1a), PEG-PAsp(DET) (Figure 1b), PAsp(DET) with DP = 92 (Figure 1c), and PAsp(DET) with DP = 225 (Figure 1d). Diameter and ζ-potential of silica-coated siRNA PICs prepared at varying sodium silicate concentrations (Figure 2). Agarose gel electrophoresis of siRNA PICs (Figure 3). Diameter of PEG-SS-PAsp(DET)/silica-coated siRNA PICs prepared at varying concentrations of PEG-SS-PAsp(DET) amine (Figure 4). Size distribution histograms of sPICs and SMAs determined by TEM images and the number statistics of DLS (Figure 5). TEM image of SMAs obtained with JEM-1400 (JEOL Ltd., Tokyo, Japan) (Figure 6). Time-dependent change in size of NPC and NDC in 10 mM HEPES buffer containing 150 mM NaCl (Figure 7). Gene silencing efficiency in A549-Luc and SKOV3-Luc cells (Figure 8). These materials are available free of charge *via* the Internet at http://pubs.acs.org.

REFERENCES AND NOTES

1. Whitehead, K. A.; Langer, R.; Anderson, D. G. Knocking Down Barriers: Advances in siRNA Delivery. *Nat. Rev. Drug Discovery* **2009**, *8*, 129–138.
2. Davidson, B. L.; McCray, P. B. Current Prospects for RNA Interference-Based Therapies. *Nat. Rev. Genet.* **2011**, *12*, 329–340.
3. Itaka, K.; Kanayama, N.; Nishiyama, N.; Jang, W.-D.; Yamasaki, Y.; Nakamura, K.; Kawaguchi, H.; Kataoka, K. Supramolecular Nanocarrier of siRNA from PEG-Based Block Catiomer Carrying Diamine Side Chain with Distinctive pK_a Directed to Enhance Intracellular Gene Silencing. *J. Am. Chem. Soc.* **2004**, *126*, 13612–13613.
4. Schiffelers, R. M.; Ansari, A.; Xu, J.; Zhou, Q.; Tang, Q.; Storm, G.; Molema, G.; Lu, P. Y.; Scaria, P. V.; Woodle, M. C. Cancer siRNA Therapy by Tumor Selective Delivery with Ligand-Targeted Sterically Stabilized Nanoparticle. *Nucleic Acids Res.* **2004**, *32*, e149.
5. Mao, S. R.; Neu, M.; Germershaus, O.; Merkel, O.; Sitterberg, J.; Bakowsky, U.; Kissel, T. Influence of Polyethylene Glycol Chain Length on the Physicochemical and Biological Properties of Poly(ethylene imine)-graft-poly(ethylene glycol) Block Copolymer/siRNA Polyplexes. *Bioconjugate Chem.* **2006**, *17*, 1209–1218.
6. Heidel, J. D.; Yu, Z. P.; Liu, J. Y. C.; Rele, S. M.; Liang, Y. C.; Zeidan, R. K.; Kornbrust, D. J.; Davis, M. E. Administration in Non-human Primates of Escalating Intravenous Doses of Targeted Nanoparticles Containing Ribonucleotide Reductase Subunit M2 siRNA. *Proc. Natl. Acad. Sci. U. S. A.* **2007**, *104*, 5715–5721.
7. Kumar, P.; Wu, H.; McBride, J. L.; Jung, K.-E.; Kim, M. H.; Davidson, B. L.; Lee, S. K.; Shankar, P.; Manjunath, N. Transvascular Delivery of Small Interfering RNA to the Central Nervous System. *Nature* **2007**, *448*, 39–45.
8. Kim, S. H.; Jeong, J. H.; Lee, S. H.; Kim, S. W.; Park, T. G. Local and Systemic Delivery of VEGF siRNA Using Polyelectrolyte Complex Micelles for Effective Treatment of Cancer. *J. Controlled Release* **2008**, *129*, 107–116.
9. Matsumoto, S.; Christie, R. J.; Nishiyama, N.; Miyata, K.; Ishii, A.; Oba, M.; Koyama, H.; Yamasaki, Y.; Kataoka, K. Environment-Responsive Block Copolymer Micelles with a Disulfide Cross-linked Core for Enhanced siRNA Delivery. *Biomacromolecules* **2009**, *10*, 119–127.
10. Schaffert, D.; Troiber, C.; Salcher, E. E.; Frohlich, T.; Martin, I.; Badgujar, N.; Dohmen, C.; Edinger, D.; Klager, R.; Maiwald, G.; *et al.* Solid-phase Synthesis of Sequence-defined T-, i-, and U-shape Polymers for pDNA and siRNA Delivery. *Angew. Chem., Int. Ed.* **2011**, *50*, 8986–8989.
11. Siegwart, D. J.; Whitehead, K. A.; Nuhn, L.; Sahay, G.; Cheng, H.; Jiang, S.; Ma, M.; Lytton-Jean, A.; Vegas, A.; Fenton, P.; *et al.* Combinatorial Synthesis of Chemically Diverse Core-Shell Nanoparticles for Intracellular Delivery. *Proc. Natl. Acad. Sci. U. S. A.* **2011**, *108*, 12996–13001.
12. Suma, T.; Miyata, K.; Ishii, T.; Uchida, S.; Uchida, H.; Itaka, K.; Nishiyama, N.; Kataoka, K. Enhanced Stability and Gene Silencing Ability of siRNA-Loaded Polyion Complexes Formulated from Polyaspartamide Derivatives with a Repetitive Array of Amino Groups in the Side Chain. *Biomaterials* **2012**, *33*, 2770–2779.
13. Morrissey, D. V.; Lockridge, J. A.; Shaw, L.; Blanchard, K.; Jensen, K.; Breen, W.; Hartsough, K.; Machemer, L.; Radka, S.; Jadhav, V.; *et al.* Potent and Persistent *in Vivo* Anti-HBV Activity of Chemically Modified siRNA. *Nat. Biotechnol.* **2005**, *23*, 1002–1007.
14. Nakamura, Y.; Kogure, K.; Futaki, S.; Harashima, H. Octaarginine-Modified Multifunctional Envelope-Type Nano Device for siRNA. *J. Controlled Release* **2007**, *119*, 360–367.
15. Akinc, A.; Zumbuehl, A.; Goldberg, M.; Leshchiner, E. S.; Busini, V.; Ossain, N.; Bacallado, S. A.; Nguyen, D. N.; Fuller, J.; Alvarez, R.; *et al.* A Combinatorial Library of Lipid-like Materials for Delivery of RNAi Therapeutics. *Nat. Biotechnol.* **2008**, *26*, 561–569.
16. Xia, T.; Kovochich, M.; Liong, M.; Meng, H.; Kabehie, S.; George, S.; Zink, J. I.; Nel, A. E. Polyethyleneimine Coating Enhances the Cellular Uptake of Mesoporous Silica

Nanoparticles and Allows Safe Delivery of siRNA and DNA Constructs. *ACS Nano* **2009**, *3*, 3273–3286.
17. Chen, A. M.; Zhang, M.; Wel, D. G.; Stueber, D.; Taratula, O.; Minko, T.; He, H. X. Co-delivery of Doxorubicin and Bcl-2 siRNA by Mesoporous Silica Nanoparticle Enhances the Efficacy of Chemotherapy in Multidrug-Resistant Cancer Cells. *Small* **2009**, *5*, 2673–2677.
18. Kakizawa, Y; Furukawa, S; Kataoka, K. Block Copolymer-Coated Calcium Phosphate Nanoparticles Sensing Intracellular Environment for Oligodeoxynucleotide and siRNA Delivery. *J. Controlled Release* **2004**, *97*, 345–356.
19. Pittella, F.; Zhang, M.; Lee, Y.; Kim, H. J.; Tockary, T.; Osada, K.; Ishii, T.; Miyata, K.; Nishiyama, N.; Kataoka, K. Enhanced Endosomal Escape of siRNA-Incorporating Hybrid Nanoparticles from Calcium Phosphate and PEG-Block Charge-Conversional Polymer for Efficient Gene Knockdown with Negligible Cytotoxicity. *Biomaterials* **2011**, *32*, 3106–3114.
20. Giljohann, D. A.; Seferos, D. S.; Prigodich, A. E.; Patel, P. C.; Mirkin, C. A. Gene Regulation with Polyvalent siRNA-Nanoparticle Conjugates. *J. Am. Chem. Soc.* **2009**, *131*, 2072–2073.
21. Lee, J. S.; Gree, J. J.; Love, K. T.; Sunshine, J.; Langer, R.; Anderson, D. G. Gold, Poly(beta-amino ester) Nanoparticles for Small Interfering RNA Delivery. *Nano Lett.* **2009**, *9*, 2402–2406.
22. Decher, G. Fuzzy Nanoassemblies: Toward Layered Polymeric Multicomposites. *Science* **1997**, *277*, 1232–1237.
23. Becker, A. L.; Johnston, A. P. R.; Caruso, F. Layer-by-Layer-Assembled Capsules and Films for Therapeutic Delivery. *Small* **2010**, *6*, 1836–1852.
24. Davila-Ibanez, A. B.; Salgueirino, V.; Martinez-Zorzano, V.; Marino-Fernandez, R.; Gracia-Lorenzo, A.; Maceira-Campos, M.; Munoz-Ubeda, M.; Junquera, E.; Aicart, E.; Rivas, J.; *et al.* Magnetic Silica Nanoparticle Cellular Uptake and Cytotoxicity Regulated by Electrostatic Polyelectrolytes–DNA Loading at Their Surface. *ACS Nano* **2012**, *6*, 747–759.
25. Elbakry, A.; Zaky, A.; Liebl, R.; Rachel, R.; Goepferich, A.; Breunig, M. Layer-by-Layer Assembled Gold Nanoparticles for siRNA Delivery. *Nano Lett.* **2009**, *9*, 2059–2064.
26. Guo, S.; Huang, Y.; Jiang, Q.; Sun, Y.; Deng, L.; Liang, Z.; Du, Q.; Xing, J.; Zhao, Y.; Wang, P. C.; *et al.* Enhanced Gene Delivery and siRNA Silencing by Gold Nanoparticles Coated with Charge-Reversal Polyelectrolyte. *ACS Nano* **2010**, *4*, 5505–5511.
27. Becker, A. L.; Orlotti, N. I.; Folini, M.; Cavalieri, F.; Zelikin, A. N.; Johnston, A. P. R.; Zaffaroni, N.; Caruso, F. Redox-Active Polymer Microcapsules for the Delivery of a Survivin-Specific siRNA in Prostate Cancer Cells. *ACS Nano* **2011**, *5*, 1335–1344.
28. Coradin, T.; Livage, J. Aqueous Silicates in Biological Sol-Gel Applications: New Perspectives for Old Precursors. *Acc. Chem. Res.* **2007**, *40*, 819–826.
29. Miyata, K.; Gouda, N.; Takemoto, H.; Oba, M.; Lee, Y.; Koyama, H.; Yamasaki, Y.; Itaka, K.; Nishiyama, N.; Kataoka, K. Enhanced Transfection with Silica-Coated Polyplexes Loading Plasmid DNA. *Biomaterials* **2010**, *31*, 4764–4770.
30. Kataoka, K.; Harada, A.; Nagasaki, Y. Block Copolymer Micelles for Drug Delivery: Design, Characterization and Biological Significance. *Adv. Drug Delivery Rev.* **2001**, *47*, 113–131.
31. Miyata, K.; Christie, R. J.; Kataoka, K. Polymeric Micelles for Nano-scale Drug Delivery. *React. Funct. Polym.* **2011**, *71*, 227–234.
32. Nomoto, T.; Matsumoto, Y.; Miyata, K.; Oba, M.; Fukushima, S.; Nishiyama, N.; Yamasoba, T.; Kataoka, K. *In Situ* Quantitative Monitoring of Polyplexes and Polyplex Micelles in the Blood Circulation Using Intravital Real-Time Confocal Laser Scanning Microscopy. *J. Controlled Release* **2011**, *151*, 104–109.
33. Takae, S.; Miyata, K.; Oba, M.; Ishii, T.; Nishiyama, N.; Itaka, K.; Yakasaki, Y.; Koyama, H.; Kataoka, K. PEG-Detachable Polyplex Micelles Based on Disulfide-Linked Block Catiomers as Bioresponsive Nonviral Gene Vectors. *J. Am. Chem. Soc.* **2008**, *130*, 6001–6009.
34. Kim, H. J.; Oba, M.; Pittella, F.; Nomoto, T.; Cabral, H.; Matsumoto, Y.; Miyata, K.; Nishiyama, N.; Kataoka, K. PEG-Detachable Cationic Polyaspartamide Derivatives Bearing Stearoyl Moieties for Systemic siRNA Delivery toward Subcutaneous BxPC3 Pancreatic Tumor. *J. Drug Target.* **2012**, *20*, 33–42.
35. Walker, G. F.; Fella, C.; Pelisek, J.; Fahrmeir, J.; Boeckle, S.; Ogris, M.; Wagner, E. Toward Synthetic Viruses: Endosomal pH-Triggered Deshielding of Targeted Polyplexes Greatly Enhances Gene Transfer *in Vitro* and *in Vivo*. *Mol. Ther.* **2005**, *11*, 418–425.
36. Saito, G.; Swanson, J. A.; Lee, K.-D. Drug Delivery Strategy Utilizing Conjugation *via* Reversible Disulfide Linkages: Role and Site of Cellular Reducing Activities. *Adv. Drug Delivery Rev.* **2003**, *55*, 199–215.
37. Corti, A.; Franzini, M.; Paolicchi, A.; Pompella, A. Gamma-glutamyltransferase of Cancer Cells at the Crossroads of Tumor Progression, Drug Resistance and Drug Targeting. *Anticancer Res.* **2010**, *30*, 1169–1181.
38. Miyata., K.; Nishiyama, N.; Kataoka, K. Rational Design of Smart Supramolecular Assemblies for Gene Delivery: Chemical Challenges in the Creation of Artificial Viruses. *Chem. Soc. Rev.* **2012**, *41*, 2562–2574.
39. Kanayama, N.; Fukushima, S.; Nishiyama, N.; Itaka, K.; Jang, W.-D.; Miyata, K.; Yamasaki, Y.; Chung, U.-I.; Kataoka, K. A PEG-Based Biocompatible Block Catiomer with High Buffering Capacity for the Construction of Polyplex Micelles Showing Efficient Gene Transfer toward Primary Cells. *ChemMedChem* **2006**, *1*, 439–444.
40. Miyata, K.; Oba, M.; Nakanishi, M.; Fukushima, S.; Yamasaki, Y.; Koyama, H.; Nishiyama, N.; Kataoka, K. Polyplexes from Poly(aspartamide) Bearing 1,2-Diaminoethane Side Chains Induce pH-Selective Endosomal Membrane Destabilization with Amplified Transfection and Negligible Cytotoxicity. *J. Am. Chem. Soc.* **2008**, *130*, 16287–16294.
41. Itaka, K.; Ishii, T.; Hasegawa, Y.; Kataoka, K. Biodegradable Polyamino Acid-Based Polycations as Safe and Effeictive Gene Carrier Minimizing Cumulative Toxicity. *Biomaterials* **2010**, *31*, 3707–3714.
42. Uchida, H.; Miyata, K.; Oba, M.; Ishii, T.; Suma, T.; Itaka, K.; Nishiyama, N.; Kataoka, K. Odd-Even Effect of Repeating Aminoethylene Units in the Side Chain of N-Substituted Polyaspartamides on Gene Transfection Profiles. *J. Am. Chem. Soc.* **2011**, *133*, 15524–1532.
43. Takemoto, H.; Ishii, A.; Miyata, K.; Nakanishi, M.; Oba, M.; Ishii, T.; Yamasaki, Y.; Nishiyama, N.; Kataoka, K. Polyion Complex Stability and Gene Silencing Efficiency with a siRNA-Grafted Polymer Delivery System. *Biomaterials* **2010**, *31*, 8097–8105.
44. Kim, H. J.; Ishii, A.; Miyata, K.; Lee, Y.; Wu, S.; Oba, M.; Nishiyama, N.; Kataoka, K. Introduction of Stearoyl Moieties into a Biocompatible Cationic Polyaspartamide Derivative, PAsp(DET), with Endosomal Escaping Function for Enhanced siRNA-Mediated Gene Knockdown. *J. Controlled Release* **2010**, *145*, 141–148.
45. Fleming, B. A. Kinetics of Reaction between Silicic Acid and Amorphous Silica Surface in NaCl Solutions. *J. Colloid Interface Sci.* **1986**, *110*, 40–64.
46. Han, M.; Bae, Y.; Nishiyama, N.; Miyata, K.; Oba, M.; Kataoka, K. Transfection Study Using Multicellular Tumor Spheroids for Screening Non-viral Polymeric Gene Vectors with Low Cytotoxicity and High Transfection Efficiencies. *J. Controlled Release* **2007**, *121*, 38–48.
47. Mislick, K. A.; Baldeshwieler, J. D. Evidence for the Role of Proteoglycans in Cation-mediated Gene Transfer. *Proc. Natl. Acad. Sci. U. S. A.* **1996**, *93*, 12349–12354.
48. He, C.; Hu, Y.; Yin, L.; Tang, C.; Yin, C. Effects of Particle Size and Surface Charge on Cellular Uptake and Biodistribution of Polymeric Nanoparticles. *Biomaterials* **2010**, *31*, 3657–3666.
49. Ferrara, N. VEGF as a Therapeutic Target in Cancer. *Oncology* **2005**, *69*, 11–16.
50. Takei, Y.; Kadomatsu, K.; Yuzawa, Y.; Matsuo, S.; Muramatsu, T. A Small Interfering RNA Targeting Vascular Endothelial Growth Factor as Cancer Therapeutics. *Cancer Res.* **2004**, *64*, 3365–3370.

51. Kim, S. H.; Jeong, J. H.; Lee, S. H.; Kim, S. W.; Park, T. G. Local and Systemic Delivery of VEGF SiRNA Using Polyelectrolyte Complex Micelles for Effective Treatment of Cancer. *J. Controlled Release* **2008**, *129*, 107–116.
52. Pittella, F.; Miyata, K.; Maeda, Y.; Suma, T.; Watanabe, S.; Chen, Q.; Christie, R. J.; Osada, K.; Nishiyama, N.; Kataoka, K. Pancreatic Cancer Therapy by Systemic Administration of VEGF siRNA Contained in Calcium Phosphate/Charge-Conversional Polymer Hybrid Nanoparticles. *J. Controlled Release* **2012**, *161*, 868–874.
53. Christie, R. J.; Matsumoto, Y.; Miyata, K.; Nomoto, T.; Fukushima, S.; Osada, K.; Halnaut, J.; Pittella, F.; Kim, H. J.; Nishiyama, N.; *et al.* Targeted Polymeric Micelles for SiRNA Treatment of Experimental Cancer by Intravenous Injection. *ACS Nano* **2012**, *6*, 5174–5189.

Journal of Controlled Release 161 (2012) 868–874

Contents lists available at SciVerse ScienceDirect

Journal of Controlled Release

journal homepage: www.elsevier.com/locate/jconrel

Pancreatic cancer therapy by systemic administration of VEGF siRNA contained in calcium phosphate/charge-conversional polymer hybrid nanoparticles

Frederico Pittella [a,b], Kanjiro Miyata [a], Yoshinori Maeda [b], Tomoya Suma [b], Sumiyo Watanabe [a], Qixian Chen [c], R. James Christie [a], Kensuke Osada [c], Nobuhiro Nishiyama [a], Kazunori Kataoka [a,b,c,d,*]

[a] Division of Clinical Biotechnology, Center for Disease Biology and Integrative Medicine, Graduate School of Medicine, The University of Tokyo, 7-3-1 Hongo, Bunkyo-ku, Tokyo 113-0033, Japan
[b] Department of Bioengineering, Graduate School of Engineering, The University of Tokyo, 7-3-1 Hongo, Bunkyo-ku, Tokyo 113-8656, Japan
[c] Department of Materials Engineering, Graduate School of Engineering, The University of Tokyo, 7-3-1 Hongo, Bunkyo-ku, Tokyo 113-8656, Japan
[d] Center for NanoBio Integration, The University of Tokyo, 7-3-1 Hongo, Bunkyo-ku, Tokyo 113-8656, Japan

ARTICLE INFO

Article history:
Received 16 February 2012
Accepted 1 May 2012
Available online 11 May 2012

Keywords:
siRNA
Calcium phosphate
Nanoparticle
VEGF
PEG
Charge-conversional polymer

ABSTRACT

Development of an efficient *in vivo* delivery vehicle of small interfering RNA (siRNA) is the key challenge for successful siRNA-based therapies. In this study, toward systemic delivery of siRNA to solid tumors, a smart polymer/calcium phosphate (CaP)/siRNA hybrid nanoparticle was prepared to feature biocompatibility, reversible stability and endosomal escape functionality using a pH sensitive block copolymer of poly(ethylene glycol) and charge-conversional polymer (PEG-CCP), of which anionic functional groups could be converted to cationic groups in an endosomal acidic condition for facilitated endosomal escape. Nanoparticles were confirmed to be approximately 100 nm in size, narrowly dispersed and spherical. Also, the nanoparticle was highly tolerable in medium containing serum, while releasing the entrapped siRNA in a cytoplasm-mimicking ionic condition, presumably based on the equilibrium between CaP complexes and calcium ions. Further, the nanoparticle showed high gene silencing efficiency in cultured pancreatic cancer cells (BxPC3) without associated cytotoxicity. Ultimately, systemic administration of the nanoparticles carrying vascular endothelium growth factor (VEGF) siRNA led to the significant reduction in the subcutaneous BxPC3 tumor growth, well consistent with the enhanced accumulation of siRNA and the significant VEGF gene silencing (~68%) in the tumor. Thus, the hybrid nanoparticle was demonstrated to be a promising formulation toward siRNA-based cancer therapies.

1. Introduction

Since elucidation of the molecular pathway of ribonucleic acid interference (RNAi) [1], small interfering ribonucleic acid (siRNA) has emerged as a potential therapeutic agent for modulating the production of proteins associated with disease [2,3]. Several clinical trials employing siRNA-based cancer therapies are currently ongoing [3,4]. In many cases, siRNA has been applied with a delivery vehicle to facilitate accumulation within the therapeutic site of activity (cell cytoplasm). Incorporation of siRNA within delivery vehicles is performed to overcome barriers associated with transport of this fragile and highly anionic macromolecule, such as premature degradation by RNases and inefficient cellular internalization. Therefore, development of more effective delivery vehicles is currently a major challenge for improving siRNA therapies.

Calcium phosphate (CaP)-based nanoparticles are a promising siRNA delivery platform because of the fact that CaP is naturally generated in the body (thus well tolerated), and also encapsulates negatively charged molecules during precipitation [5,6]. In this regard, a strategy to control the growth of CaP/siRNA precipitates is essential for their utilization toward systemic delivery applications. Several previous studies, including ours, have developed successful strategies to control nanoparticle size on the order of several tens to one hundred nanometer by coating with poly(ethylene glycol) (PEG)-*b*-polyanions [7–10], PEG-functionalized bisphosphonate [11], lipid bilayer membranes [12], or even nucleic acids [13]. Notably, a PEG shell on the nanoparticle surface has the desirable functionality to reduce non-specific interactions with biomacromolecules in the bloodstream, termed stealth property, for improved pharmacokinetics as well as facilitated accumulation in solid tumors through enhanced permeability and retention (EPR) effect [14–17].

Once internalized by cells via endocytosis, nanoparticles are transported to endosomal compartments ultimately lysosome where they remain until degraded. To overcome the endosomal/lysosomal entrapment of CaP nanoparticles, we developed CaP/polymer hybrid

* Corresponding author at: Division of Clinical Biotechnology, Center for Disease Biology and Integrative Medicine, Graduate School of Medicine, The University of Tokyo, 7-3-1 Hongo, Bunkyo-ku, Tokyo 113-0033, Japan.
E-mail address: kataoka@bmw.t.u-tokyo.ac.jp (K. Kataoka).

0168-3659/$ – see front matter © 2012 Elsevier B.V. All rights reserved.
doi:10.1016/j.jconrel.2012.05.005

nanoparticles containing functionality designed to promote escape from these subcellular compartments. This was achieved using a block copolymer of PEG and an endosome-disrupting polyanion, poly(*N*″-{*N*′-[(*N*-*cis*-aconityl)-2-aminoethyl]-2-aminoethyl}aspartamide) (PAsp(DET-Aco)) [18]. PAsp(DET-Aco) is relatively stable at the extracellular pH of 7.4 but degrades at pH ~5.5 (lysosome pH) by cleavage of *cis*-aconitic amide linkages, thus reverting back to the parent polycation, PAsp(DET). This degradation event results in conversion of the polymer charge from anionic to cationic, and is thus termed a charge-conversional polymer (CCP) (Fig. 1) [19]. PAsp(DET) has been shown to exhibit a distinctive change in the structure of side chains between pH 7.4 and pH 5.5 due to protonation of amino groups, i.e., monoprotonated diaminoethane at pH 7.4 and diprotonated diaminoethane at pH 5.5, allowing pH-selective membrane disruption for efficient endosomal escape of nucleic acids without associated toxicity [20–25]. In addition, PEG-PAsp(DET-Aco) was confirmed to facilitate excellent colloidal dispersion of CaP nanoparticles, while also improving the endosomal escape of siRNA, resulting in efficient gene silencing to cultured pancreatic carcinoma cells (PanC-1) [18].

The present work reports the *in vivo* application of the CaP/block copolymer/siRNA hybrid nanoparticles prepared with PEG-PAsp(DET-Aco) for treatment of subcutaneous pancreatic tumor (BxPC3) models in mice by systemic administration. Removal of free calcium ions from CaP nanoparticle solutions is critical for its systemic administration, as excess calcium ions may induce adverse effects in the bloodstream [32]. Thus nanoparticle solutions were purified by ultrafiltration, and then characterized with non-purified controls in terms of stability, morphology, calcium amount and biological activity. For treatment of subcutaneous pancreatic tumors, the key pro-angiogenic molecule vascular endothelial growth factor (VEGF) was selected as the target gene, once it is known to be over-expressed in many cancerous cells, promoting angiogenesis through endothelial proliferation, survival and migration [26]. Moreover, silencing of the VEGF signaling pathway has been shown to suppress tumor angiogenesis and growth [27–30]. After systemic administration of purified nanoparticles incorporating VEGF siRNA for anti-angiogenic therapy, the accumulation of siRNA and the expression level of VEGF mRNA in the tumor tissue were evaluated to elucidate their correlation with tumor growth rates. This work demonstrates significant antitumor activity induced by VEGF gene silencing with siRNA delivered by CaP/block copolymer hybrid nanoparticles.

2. Materials and methods

2.1. Materials, cell line and animals

Dulbecco's modified eagle's medium (DMEM) without L-glutamine and phenol red, RPMI 1640 and *cis*-aconitic anhydride were purchased from Sigma-Aldrich (St. Louis, MO). α-Methoxy-ω-amino poly(ethylene glycol) (MeO–PEG–NH_2) (M_w: 12,000) and β-benzyl-L-aspartate *N*-carboxy anhydride (BLA-NCA) were obtained from NOF Co., Inc. (Tokyo, Japan) and Chuo Kaseihin Co., Inc. (Tokyo, Japan), respectively. *N*-methyl-2-pyrrolidone (NMP), diethylenetriamine (DET), dimethyl sulfoxide (DMSO), *N*,*N*-dimethylformamide (DMF), dichloromethane (DCM) and acetic anhydride were purchased from Tokyo Chemical Industry Co. Ltd. (Tokyo, Japan) or Nacalai Tesque (Tokyo, Japan), and used after conventional distillation. Acetic acid, acetonitrile, acetone, diethyl ether and hydrochloric acid were purchased from Wako Pure Chemical Industries Ltd. (Osaka, Japan). Fetal bovine serum (FBS) was purchased from Dainippon Sumitomo Pharma Co., Ltd. (Osaka, Japan). RT-PCR primers used for human actin and human VEGF were synthesized by Hokkaido System Science (Hokkaido, Japan) and the sequences are the following: CCAACCGCGAGAAGATGA (actin forward); CCAGAGGCGTACAGGGATAG (actin reverse); AGTGGTCCCAGGCTGCAC (VEGF forward); TCCATGAACTTCACCACTTCGT (VEGF reverse). All the siRNAs were synthesized by Hokkaido System Science (Hokkaido, Japan). The sequences of VEGF siRNA (siVEGF) are 5′-GGAGUACCCUGAUGAGAUCdTdT-3′ (sense) and 5′-GAUCUCAUCAGGGUACUCCdTdT-3′ (antisense), and the sequences of scramble siRNA (siSCR) are 5′-UUCUCCGAACGUGUCACGUdTdT-3′ (sense); 5′-ACGUGACACGUUCGGAGAAdTdT-3′ (antisense).

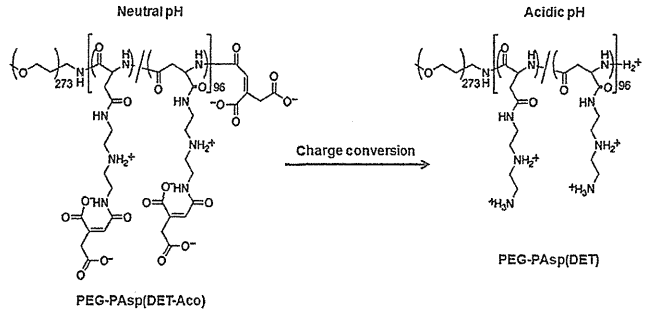

Fig. 1. Change in the chemical structure of PEG-PAsp(DET-Aco) to PEG-PAsp(DET) in response to the acidic pH.

BxPC3 cells (human tumorigenic pancreatic adenocarcinoma, ATCC number: CRL-1687) were obtained from the American Type Culture Collection (Manassas, VA). Cells were maintained in RPMI 1640 medium (Sigma Chemical Co., Inc.) containing 10% fetal bovine serum (FBS) in a humidified atmosphere containing 5% CO_2 at 37 °C. Balb-c nu/nu mice (female; 18–20 g body weight; age, 6 weeks) were purchased from Charles River Japan (Kanagawa, Japan). All animal experiments were performed in accordance with the Guidelines for the Care and Use of Laboratory Animals as stated by the University of Tokyo.

2.2. Polymer synthesis

Detailed synthesis methods of the parent polycation PEG-PAsp(DET) and PEG-PAsp(DET-Aco) derivative are described in Supplementary data.

2.3. Preparation of PEG-CCP/siRNA/CaP hybrid nanoparticles

A solution of 2.5 M $CaCl_2$ (1 μL) was diluted in 10 mM Tris buffer (pH 10) (11.5 μL). Another solution containing PEG-PAsp(DET-Aco) (1.0 mg/mL) in 10 mM Tris/HCl buffer (pH 7.5) was mixed with a solution of 15 μM siRNA in 10 mM HEPES buffer (pH 7.2) and with 50 mM HEPES buffer containing 1.5 mM Na_3PO_4 and 140 mM NaCl (pH 7.5) (2.5 μL: 5 μL: 5 μL). The former solution was mixed with the latter solution by pipetting for around 20 s (final siRNA concentration; 3 μM).

2.4. Purification of PEG-CCP/siRNA/CaP hybrid nanoparticles

The purification of hybrid nanoparticles for removal of excess amount of free calcium ions was carried out immediately after preparation. PEG-CCP/siRNA/CaP hybrid nanoparticle solution containing 41.3 μg siRNA and 150 μg PEG-CCP (1 mL) was added to a VivaSpin-06 device (MWCO: 10 kDa) containing 1 mL of an extracellular (EC) buffer that mimics the ionic strength of extracellular environment (2 mM $CaCl_2$, 1 mM Na_2HPO_4, 25 mM Tris and 140 mM NaCl at pH 7.4) [8]. The mixture was centrifuged in a swing bucket rotor at 900 g and 4 °C for 20 min. To minimize non-specific binding of nanoparticles to the membrane, the centrifuge filter devices were washed with de-ionized water before use. After centrifugation, the retained solution was collected and used in further experiments.

2.5. Determination of calcium content in nanoparticles

The total calcium content present in the solution of non-purified and purified/concentrated hybrid nanoparticles was determined by the SRL Laboratories (SRL Inc., Tokyo, Japan) through spectrophotometry using

arsenazo III. All the samples were diluted four times with distilled water to the final volume of 300 μL before assay. The reaction of arsenazo III dye with calcium under acidic conditions produces a blue–purple complex, of which concentration is determined spectrophotometrically at the wavelength of 660 nm. Obtained values were used to calculate the efficiency of calcium removal from nanoparticle solution.

2.6. Dynamic light scattering (DLS) measurements

DLS measurements were carried out at 25 °C using a Zetasizer Nano ZS (Malvern Instruments, UK) at a detection angle of 173° with a He–Ne laser (633 nm) as the incident beam. The data obtained from the rate of decay in the photon correlation function were analyzed with a cumulant method to obtain the corresponding hydrodynamic diameters and polydispersity indices (PdI) (μ/G^2) of the nanoparticles. The colloidal stability of both purified and non-purified nanoparticles was monitored during several days and the result was presented as a relative size to the initial hydrodynamic diameter obtained in the first day.

2.7. Atomic force microscopy (AFM) imaging

AFM imaging of the nanoparticles was performed using a MMAFM, Nanoscope V (Bruker AXS, Madison, WI) in ScanAsyst Atomic Force Microscopy Imaging mode with standard silicon probes. Imaging was conducted under air on a highly orientated pyrolytic graphite (HOPG) substrate. The obtained images were processed by flattening to remove the background slope of the substrate surface.

2.8. Fluorescence correlation spectroscopy (FCS) measurements

FCS measurements were performed using a Confocor3 module (Carl Zeiss, Jena, Germany) equipped with a Zeiss C-Apochromat 40× water objective. Samples prepared with Cy5-labeled siRNA were measured with the excitation of a He–Ne laser (633 nm, 5 mW) and the emission passed through a 650 nm long pass filter. Samples were placed into 8-well Lab-Tek chambered borosilicate cover-glass slides (Nalge Nunc International, Rochester, NY). Determination of the focal volume was established by calibration with 10 nM Cy5 standard solution. Each analysis consisted of 10 measurements with a sampling time of 20 s and the measured autocorrelation curves were fitted with the Zeiss Confocor3 software package to obtain the diffusion coefficient. The stability of nanoparticles under a cell culture condition was evaluated after dilution of samples with DMEM containing 10% FBS without L-glutamine and phenol red and then incubation at 37 °C. The stability of nanoparticles in the solution mimicking the intracellular fluids was evaluated after dilution of the samples with the ionic solution ($CaCl_2$ 100 nM, Na_2HPO_4 40 mM, NaCl 140 mM, pH 7.4), as previously described [8]. The concentration of Cy5-labeled siRNA was adjusted to 100 nM, corresponding to the *in vitro* gene silencing experiment.

2.9. In vitro gene silencing

To evaluate the gene silencing efficiency of the purified nanoparticles compared to non-purified controls, BxPC3 cells were seeded with 2 mL of RPMI 1640 containing 10% FBS on a 6 well plate at 5×10^4 cells/well. After 24 h, nanoparticle solutions were added with fresh medium (100 nM siRNA). After another 24 h, cells were harvested and RNA was extracted using RNeasy Mini Kit (Qiagen, Valencia, CA), according to the manufacturer's instruction.

2.10. Real-time reverse transcriptional (RT)-PCR

After obtaining the RNA from cells or tissue, the RNA concentration was measured and then sample concentrations were normalized. Next, the genomic DNA elimination was performed prior to cDNA synthesis using a QuantiTect Reverse Transcription kit (Qiagen, Valencia, CA). Real-time RT-PCR was performed using an ABI 7500 Fast Real-time RT-PCR System (Applied Biosystems, Foster City, CA) and QuantiTect SYBR Green PCR Master Mix (Qiagen, Valencia, CA). Actin was used as the house-keeper gene and the obtained data were normalized before statistical analysis.

2.11. Antitumor activity

Balb/c nude mice (female, 6 week old) were subcutaneously implanted with BxPC3 tumor (3 mm×3 mm×1 mm). The tumors were allowed to grow for 3 weeks before sample injection. Further, the mice bearing tumors with similar volume (~50 mm^3) were randomly distributed in groups ($n=4$). Thereafter, hybrid nanoparticles loading siVEGF (25 μg siRNA in 200 μL per injection) were injected into the tail vein 4 times at days 2, 5, 8 and 12. Tumor size and body weight for each mouse were monitored for 13 days. The tumor volume was calculated based on a modified ellipsoidal formula [30,31]: tumor volume $= 1/2(\text{length}\times\text{width}^2)$.

2.12. Tumor accumulation

Similarly to Section 2.11, BxPC3 tumor-bearing mice were prepared by subcutaneous implantation of the tumor pieces (3 mm×3 mm×1 mm). The tumors were allowed to grow for 4 weeks before sample injection. Five mice bearing tumors of the similar volume (~70 mm^3) were randomly selected for each cohort ($n=5$). Hybrid nanoparticles containing Cy5-labeled siRNA were intravenously injected into the tail vein at 15 μg of Cy5-labeled siRNA per injection. Mice were sacrificed 60 min after injection and tumors were excised. Cy5 fluorescence from the tumor tissue was measured by IVIS (Caliper Life Sciences, Hopkinton, MA). Results were expressed as total photon counts normalized by tumor weight.

2.13. In vivo gene silencing in tumor tissue

BxPC3 tumor-bearing mice were prepared by subcutaneous implantation of the tumor pieces (3 mm×3 mm×1 mm) and then allowed to grow for 4 weeks, similar to the method described in Sections 2.11 and 2.12. Mice bearing tumors of similar volume (~70 mm^3) were randomly distributed in groups ($n=3$). Thereafter, hybrid nanoparticles loading siVEGF (25 μg siRNA in 200 μL per injection) were injected into the tail vein on days 1, 4, 8 and 34. After 24 h of the last injection, each tumor was excised and the non-necrotic part of the tumor (~20 mg) was cut into small pieces and sonicated for 10 s in a lysis buffer. The lysate was centrifuged and then the supernatant was used to extract RNA using the RNeasy Mini Kit (Qiagen, Valencia, CA), according to the manufacturer's instruction. Extracted RNA was further used to verify VEGF gene silencing by real-time RT-PCR, as described in Section 2.10.

3. Results and discussion

3.1. Preparation and purification/concentration of hybrid nanoparticles

The functional CCP block copolymer, PEG-PAsp(DET-Aco) (Fig. 1), was synthesized using a procedure similar to our previous report [18]. Successful synthesis of PEG-PAsp(DET-Aco) was confirmed from the ^{1}H NMR spectrum (Supporting Fig. 1) by the appearance of protons present on acid-labile *cis*-aconitic amide (Aco) moieties. This introduction is accompanied by the conversion of cationic charges to negative charges in the polyaspartamide side chain, enabling integration of PEG-CCP into CaP nanoparticles. The prepared charge-conversional polymer shows high stability at neutral pH but becomes cleavable at acidic pH to reproduce cationic PAsp(DET) from anionic PAsp(DET-Aco) (Fig. 1). Note that, once in the acidic environment of the endosome/lysosome, PAsp(DET) can disrupt their membrane to facilitate the escape of nanoparticles from these compartments [18,25].

PEG-CCP/CaP hybrid nanoparticles were prepared by simple mixing of the component solutions [18]. The initial solution of the prepared nanoparticles contains several ions, such as Ca^{2+}, that may perturb the normal body homeostasis when applied systemically [32], thereby requiring purification of the solution for removal of the ions before systemic administration. However, the CaP nanoparticles are likely to dissociate in lower ionic strength solutions due to an equilibrium shift [8–10]. Thus, a suitable buffer solution is necessary for maintaining nanoparticle structure after purification. Our previous work suggested that PEGylated CaP nanoparticles were tolerable to an extracellular ionic solution ($CaCl_2$ 2 mM, Na_2HPO_4 1 mM, Tris 25 mM, NaCl 140 mM, pH 7.4) as they effectively delivered siRNA into cultured cells in that solution. The calcium concentration of the extracellular ionic solution is similar to that of body fluids, suggesting that minimal perturbation to blood homeostasis following intravenous administration is expected.

Hybrid nanoparticle solutions were purified by an ultrafiltration method, which allows rapid exchange of the buffer solutions. The ultrafiltration (MWCO: 10 kDa) was performed with replacement of the original solution for nanoparticle preparation ($CaCl_2$ 100 mM, Na_3PO_4 0.3 mM, NaCl 28 mM, Tris 6.6 mM, HEPES 12 mM) with EC buffer ($CaCl_2$ 2 mM, Na_2HPO_4 1 mM, Tris 25 mM, NaCl 140 mM, pH 7.4). The arsenazo III dye-based colorimetric assay revealed that the ultrafiltration process removed 84% of the original calcium content, with residual calcium corresponding mostly to the calcium contained in nanoparticles. The resulting nanoparticles were characterized by DLS and AFM. Purified nanoparticles maintained a narrowly dispersed size distribution in the DLS (Z-weighted) histogram, similar to non-purified controls (Fig. 2A). Spherical morphologies with the similar size were observed in the AFM images of both purified and non-purified hybrid nanoparticles (Figs. 2B and C). These results indicate that purification for removal of excess calcium ions was successful, without alteration of hybrid nanoparticle structure.

Hybrid nanoparticle stability upon storage is also important for their quality control towards pharmaceutical applications. Thus, the size of hybrid nanoparticle was monitored over time by DLS following storage at 4 °C (Fig. 3). Non-purified hybrid nanoparticles did not show a significant change in both size and PdI for at least 168 h (7 days). Purified nanoparticle size remained similar to that of the non-purified control for the first 96 h and then the size slightly increased thereafter, possibly due to secondary aggregate formation. This aggregation can be explained by compromised colloidal stability of nanoparticles, triggered by PEG-CCP detachment from the nanoparticles associated with their gradual dissolution. These results suggest that the dissolution of the purified nanoparticle is intrinsically slow in the EC buffer.

3.2. Stability of hybrid nanoparticles in a serum-containing culture medium and a cytoplasmic ionic solution

Purified hybrid nanoparticle stability was further assessed in medium containing serum proteins. Nanoparticles were prepared with Cy5-labeled siRNA (Cy5-siRNA) and then subjected to fluorescence correlation spectroscopy (FCS) analysis. FCS analysis allows determination of the diffusion coefficient of siRNA-incorporating nanoparticles in the complex protein-containing solution without interference from non-labeled macromolecules or aggregates [33–35]. Note that the diffusion coefficient is inversely proportional to the hydrodynamic size of the fluorescent molecule based on the Stokes–Einstein equation for spherical particles; thus the size of nanoparticles can be determined. In conventional condition used for siRNA transfection (100 nM siRNA in 10% FBS medium), the initial size of nanoparticles was determined to be approximately 100 nm (Fig. 4A), which is consistent with the size in DLS histogram and AFM image of nanoparticles not exposed to biological media (Fig. 2). Additionally, size was maintained following 4 h incubation at 37 °C, indicating high tolerability in medium containing serum proteins.

In addition to high tolerability within extracellular conditions, delivery vehicles must finally release the encapsulated siRNA in the cytoplasm to gain access to the RNAi pathway. Hence, siRNA release from the hybrid nanoparticles was further evaluated by FCS in a solution mimicking the ionic condition of the cytoplasm ($CaCl_2$ 100 nM, Na_2HPO_4 40 mM, NaCl 140 mM, pH 7.4), as the dissolution of CaP nanoparticles should be significantly influenced by the concentration of calcium and phosphate ions. The average calcium ion concentrations are 2 mM and 100 nM in the blood and the cytoplasm, respectively. The lower calcium concentration in the cell cytoplasm may trigger selective intracellular release of siRNA from the CaP nanoparticles. Indeed, when nanoparticles were incubated in the cytoplasmic ionic solution, the size of the nanoparticles was drastically reduced within 1 h incubation, ultimately reaching the same value of naked siRNA (Fig. 4B), which is consistent with our previous findings regarding the dissolution behavior of hybrid nanoparticles [8].

3.3. In vitro gene silencing

The gene silencing activity of nanoparticles containing siVEGF was evaluated in cultured human pancreatic adenocarcinoma (BxPC3) cells. BxPC3 was chosen as a target cancer cell because of the fact that subcutaneous BxPC3 tumors exhibit poorly differentiated histology with thick fibrotic stromal tissue surrounding tumor nests [36], thereby resembling intractable tumors in clinical settings. As shown in Fig. 5, both non-purified and purified hybrid nanoparticles encapsulating siVEGF significantly reduced VEGF mRNA in comparison with controls incorporating siSCR. The reduction in VEGF mRNA was 71% and 63% for purified and non-purified nanoparticles, respectively. Strong gene silencing activity of hybrid nanoparticles is probably due to their high complex stability in the transfection medium (Fig. 4A) and selective siRNA release in the cell cytoplasm (Fig. 4B) as well as facilitated endosomal escape of siRNA by PEG-CCP, as extensively examined in previous studies [18,19]. No statistical difference was found between nanoparticle formulations, indicating that there was apparently no loss of the biological activity of siRNA after purification. Analysis of cell viability (CCK-8, Dojindo, Japan) showed no difference between nanoparticle-treated samples and controls at tested siRNA

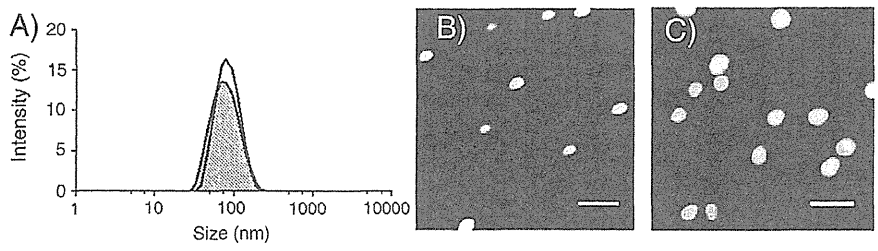

Fig. 2. (A) Size distribution of CaP nanoparticles before (filled curve) and after (open curve) purification by ultrafiltration, determined by DLS. (B, C) Atomic force microscopic images of non-purified (B) and purified (C) hybrid nanoparticles. Scale bar corresponds to 200 nm.

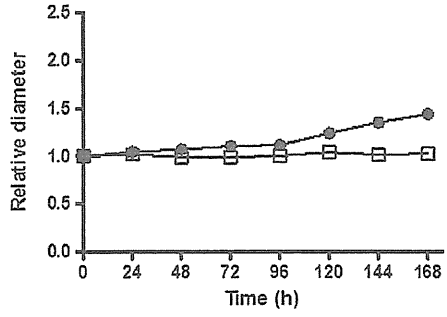

Fig. 3. Time-dependent change in the relative diameter of non-purified (open square) and purified (closed circle) hybrid nanoparticles, determined by DLS (temperature: 4 °C, siRNA concentration: 3 μM).

concentration (Supporting Fig. 2), indicating that VEGF silencing is due to the RNAi effect and not an artifact of toxicity.

3.4. Antitumor activity

Antitumor activity of siVEGF-incorporating hybrid nanoparticles was evaluated against a subcutaneous BxPC3 tumor model. Silencing of VEGF gene in tumor tissues can prevent angiogenesis, subsequently blocking the nutrient supply needed for tumor growth (antiangiogenic therapy). As presented in Fig. 6, tumors treated by I.V. injection of nanoparticles containing siVEGF showed suppressed growth, compared to those treated with nanoparticles containing siSCR as well as nanoparticles without siRNA and EC buffer only. A statistical significance was observed at days 3, 5, 7 and 9 for tumors treated with the siVEGF nanoparticles compared to controls. It is noteworthy that the significant tumor growth inhibition was observed after the first injection of the siVEGF nanoparticle. At day 9, the tumor volume in mice treated with the siVEGF nanoparticles was around 66% of the average volume of controls. I.V. injection of nanoparticles did not result in

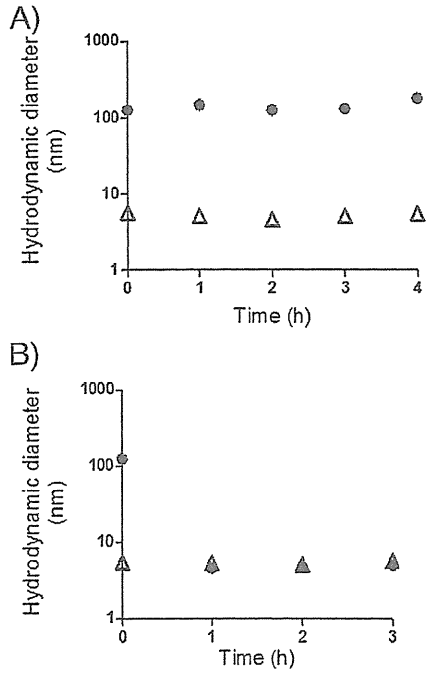

Fig. 4. Time-dependent change in hydrodynamic diameters of hybrid nanoparticles incorporating Cy5-siRNA (closed circle) and naked Cy5-siRNA (open triangle) determined by FCS in the medium containing 10% FBS (A) and in the medium mimicking the cytoplasm (Ca^{2+} and PO_4^{3-} concentrations were 100 nM and 40 mM, respectively) (B).

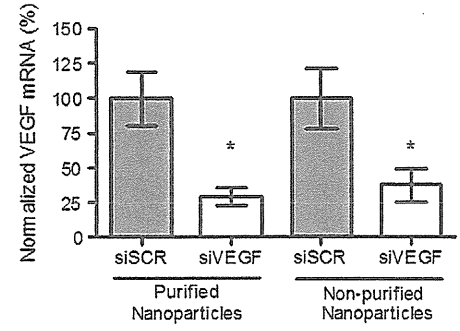

Fig. 5. Gene silencing activity of hybrid nanoparticles in cultured BxPC3 cells (siRNA concentration: 100 nM, incubation time: 24 h, $n=3$). *$p<0.05$ for the control incorporating siSCR (ANOVA followed by Newman–Keuls).

acute or severe toxicity, as no significant difference in body weight was observed between treated and control groups during the experimental period (data not shown). Additionally, blood levels of alanine aminotransferase (ALT) and aspartate aminotransferase (AST) were not significantly altered after I.V. injection of hybrid nanoparticles (Supporting Fig. 3), suggesting negligible acute toxicity associated with nanoparticle administration. These results demonstrate that the PEG-CCP/CaP hybrid nanoparticle with siVEGF is a promising formulation for cancer therapy.

3.5. Accumulation of siRNA and gene silencing in tumors

In order to obtain further evidence that the antitumor activity of siRNA-containing hybrid nanoparticles was induced by the RNAi effect, accumulation of siRNA within subcutaneous tumors was evaluated. Hybrid nanoparticles were prepared with Cy5-siRNA and injected into mice in the similar manner used for tumor growth inhibition experiments. Mice were sacrificed and the tumors were excised 60 min after systemic administration of the hybrid nanoparticles, and Cy5 fluorescence was measured by IVIS. Fluorescence intensity was normalized to the tumor weight for quantitative evaluation. Significantly stronger fluorescence was detected in tumors treated with hybrid nanoparticles, compared to naked siRNA (Fig. 7A), indicating enhanced tumor accumulation of siRNA by hybrid nanoparticle delivery. Considering the fact that naked siRNA is immediately degraded in the bloodstream and subsequently cleared from kidney, the improved tumor accumulation may be due to suppressed siRNA degradation in the bloodstream as well as slower renal clearance of siRNA.

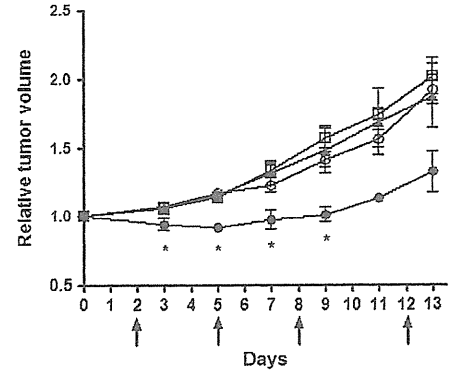

Fig. 6. Relative tumor volume of subcutaneous BxPC3 tumors treated by the hybrid nanoparticles with siVEGF (closed circle), with siSCR (closed triangle), hybrid nanoparticles without siRNA (open square) and EC buffer control (open circle) ($n=4$). Arrows indicate injection day (25 μg siRNA/injection). *$p<0.05$ for EC buffer control (ANOVA followed by Newman–Keuls).

Target gene mRNA levels were also evaluated as direct evidence for RNAi-based antitumor activity. In order to confirm VEGF mRNA degradation in tumor tissue, an additional injection of nanoparticles was performed to a separated group of mice bearing subcutaneous BxPC3 tumors ($n=3$). Approximately 1 day after the injection, mice were sacrificed and tumors were excised, followed by the extraction of RNA and real-time RT-PCR analysis. Fig. 7B clearly shows that significantly higher gene silencing activity (~68%) was achieved with hybrid nanoparticles containing siVEGF, compared to those prepared with siSCR as well as a buffer control. This result corroborates with the significant antitumor activity achieved with nanoparticles containing siVEGF (Fig. 6). Altogether, effective tumor accumulation and VEGF mRNA degradation strongly suggest that tumor growth suppression was a result of RNAi.

4. Conclusion

In this work, the *in vivo* application of PEG-CCP/CaP hybrid nanoparticles carrying siRNA was investigated for siRNA-based cancer treatment. Hybrid nanoparticles were submitted to purification for significant reduction of the amount of free calcium in solution. Purified hybrid nanoparticles were found to have the following characteristics: i) a similar size distribution and morphology to non-purified controls, ii) excellent tolerability in the serum-containing medium, iii) reversible capture of siRNA, with release in cytoplasmic ionic conditions. Efficient gene silencing activity without associated toxicity was also confirmed for nanoparticles in cultured BxPC3 cells. Intravenously injected nanoparticles incorporating VEGF siRNA led to significant reduction in tumor growth. Enhanced siRNA accumulation in subcutaneous BxPC3 tumors was found and subsequently induction of effective VEGF gene silencing in the tumor was observed. Based on the presented results, the PEG-CCP/CaP hybrid nanoparticles demonstrate great potential for clinical applications toward siRNA-based cancer therapies.

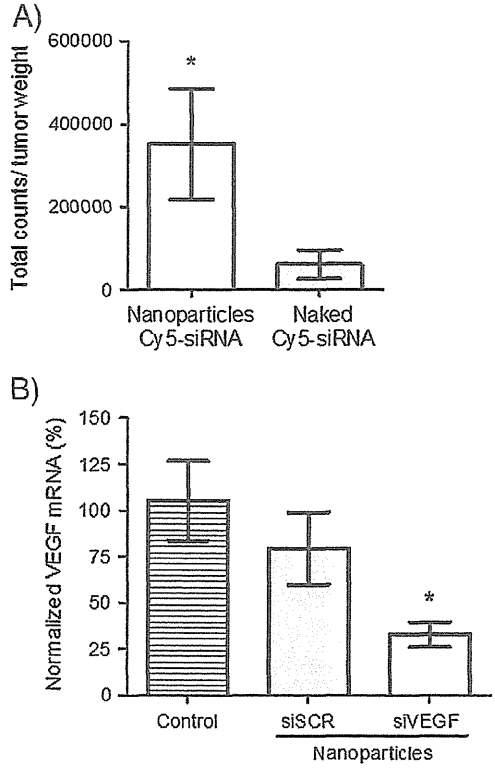

Fig. 7. (A) Accumulation of Cy5-siRNA in subcutaneous BxPC3 tumors 60 min after systemic administration. The Cy5 fluorescence intensity in the excised tumor tissue was determined by IVIS, followed by the normalization by the tumor weight ($n=5$). *$p<0.05$ for naked Cy5-siRNA (Mann–Whitney t test). (B) *In vivo* VEGF gene silencing activity in subcutaneous BxPC3 tumors 1 day after systemic administration of samples (25 μg siRNA), revealed by real-time RT-PCR ($n=3$). *$p<0.05$ for ionic buffer control (ANOVA followed by Newman–Keuls).

Acknowledgment

This research was granted by the Japan Society for the Promotion of Science (JSPS) through the "Funding Program for World-Leading Innovative R&D on Science and Technology (FIRST Program)," initiated by the Council for Science and Technology Policy (CSTP). The authors express their appreciation to Dr. M. Oba (Nagasaki University) and Dr. H. Cabral (The University of Tokyo) for the help in animal experiments.

Appendix A. Supplementary data

Supplementary data to this article can be found online at http://dx.doi.org/10.1016/j.jconrel.2012.05.005.

References

[1] A. Fire, S. Xu, M.K. Montgomery, S.A. Kostas, S.E. Driver, C.C. Mello, Potent and specific genetic interference by double-stranded RNA in *Caenorhabditis elegans*, Nature 391 (1998) 806–811.
[2] S.M. Elbashir, J. Harborth, W. Lendeckel, A. Yalcin, K. Weber, T. Tushl, Duplexes of 21-nucleotide RNAs mediate interference in cultured mammalian cells, Nature 411 (2001) 494–498.
[3] B.L. Davidson, P.B. McCray, Current prospects for RNA interference-based therapies, Nat. Rev. Genet. 12 (2011) 329–340.
[4] M.E. Davis, J.E. Zuckerman, C.H.J. Choi, D. Seligson, A. Tolcher, C.A. Alabi, Y. Yen, J.D. Heidel, A. Ribas, Evidence of RNAi in humans from systemically administered siRNA via targeted nanoparticles, Nature 464 (2010) 1067–1070.
[5] A. Maitra, Calcium phosphate nanoparticles: second-generation nonviral vectors in gene therapy, Expert. Rev. Mol. Diagn. 5 (2005) 893–905.
[6] M. Zhang, K. Kataoka, Nano-structured composites based on calcium phosphate for cellular delivery of therapeutic and diagnostic agents, Nano Today 4 (2009) 508–517.
[7] Y. Kakizawa, K. Kataoka, Block copolymer self-assembly into monodispersive nanoparticles with hybrid core of antisense DNA and calcium phosphate, Langmuir 18 (2002) 4539–4543.
[8] Y. Kakizawa, S. Furukawa, K. Kataoka, Block copolymer-coated calcium phosphate nanoparticles sensing intracellular environment for oligodeoxynucleotide and siRNA delivery, J. Control. Release 97 (2004) 345–356.
[9] Y. Kakizawa, S. Furukawa, A. Ishii, K. Kataoka, Organic–inorganic hybrid-nanocarrier of siRNA constructing through the self-assembly of calcium phosphate and PEG-based block aniomer, J. Control. Release 111 (2006) 368–370.
[10] M. Zhang, A. Ishii, N. Nishiyama, S. Matsumoto, T. Ishii, Y. Yamasaki, K. Kataoka, PEGylated calcium phosphate nanocomposites as smart environment-sensitive carriers for siRNA delivery, Adv. Mater. 21 (2009) 3520–3525.
[11] E.V. Giger, J. Puigmartí-Luis, R. Schlatter, B. Castagner, P.S. Dittrich, J.C. Leroux, Gene delivery with bisphosphonate-stabilized calcium phosphate nanoparticles, J. Control. Release 150 (2011) 87–93.
[12] J. Li, Y.C. Chen, Y.C. Tseng, C. Mozumdar, L. Huang, Biodegradable calcium phosphate nanoparticle with lipid coating for systemic siRNA delivery, J. Control. Release 142 (2010) 416–421.
[13] V.V. Sokolova, I. Radtke, R. Heumann, M. Epple, Effective transfection of cells with multi-shell calcium phosphate DNA nanoparticles, Biomaterials 27 (2006) 3147–3153.
[14] Y. Matsumura, H. Maeda, A new concept for macromolecular therapeutics in cancer-chemotherapy: mechanisms of tumoritropic accumulation of proteins and the antitumor agent SMANCS, Cancer Res. 46 (1986) 6387–6392.
[15] S.M. Moghimi, A.C. Hunter, J.C. Murray, Long-circulating and target-specific nanoparticles: theory to practice, Pharm. Rev. 53 (2001) 283–318.
[16] K. Kataoka, A. Harada, Y. Nagasaki, Block copolymer micelles for drug delivery: design, characterization and biological significance, Adv. Drug Deliv. Rev. 47 (2001) 113–131.
[17] K. Miyata, R.J. Christie, K. Kataoka, Polymeric micelles for nano-scale drug delivery, React. Funct. Polym. 71 (2011) 227–234.
[18] F. Pittella, M. Zhang, Y. Lee, H.J. Kim, T. Tockary, K. Osada, T. Ishii, K. Miyata, N. Nishiyama, K. Kataoka, Enhanced endosomal escape of siRNA-incorporating hybrid nanoparticles from calcium phosphate and PEG-block charge-conversional polymer for efficient gene knockdown with negligible cytotoxicity, Biomaterials 32 (2011) 3106–3114.
[19] Y. Lee, K. Miyata, M. Oba, T. Ishii, S. Fukushima, M. Han, H. Koyama, N. Nishiyama, K. Kataoka, Charge-conversional ternary polyplex with endosome disruption moiety: a technique for efficient and safe gene delivery, Angew. Chem. Int. Ed. 47 (2008) 5163–5166.
[20] N. Kanayama, S. Fukushima, N. Nishiyama, K. Itaka, W.D. Jang, K. Miyata, Y. Yamasaki, U.I. Chung, K. Kataoka, A PEG-based biocompatible block catiomer with high buffering capacity for the construction of polyplex micelles